

Development

Characterization of Hypothalamic MCH Neuron Development in a 3D Differentiation System of Mouse Embryonic Stem Cells

Yu Kodani,¹ Miho Kawata,¹ Hidetaka Suga,² Yoko S. Kaneko,¹ Akira Nakashima,³  Toshiki Kameyama,¹ Kanako Saito,¹ and Hiroshi Nagasaki¹

<https://doi.org/10.1523/ENEURO.0442-21.2022>

¹Department of Physiology, Fujita Health University School of Medicine, Toyoake, Aichi 470-1192, Japan, ²Department of Endocrinology and Diabetes, Nagoya University Graduate School of Medicine, Nagoya, Aichi 466-8550, Japan, and ³Department of Physiological Chemistry, Fujita Health University School of Medicine, Toyoake, Aichi 470-1192, Japan

Abstract

Hypothalamic melanin-concentrating hormone (MCH) neurons are important regulators of multiple physiological processes, such as sleep, feeding, and memory. Despite the increasing interest in their neuronal functions, the molecular mechanism underlying MCH neuron development remains poorly understood. We report that a three-dimensional culture of mouse embryonic stem cells (mESCs) can generate hypothalamic-like tissues containing MCH-positive neurons, which reproduce morphologic maturation, neuronal connectivity, and neuropeptide/neurotransmitter phenotype of native MCH neurons. Using this *in vitro* system, we demonstrate that Hedgehog (Hh) signaling serves to produce major neurochemical subtypes of MCH neurons characterized by the presence or absence of cocaine- and amphetamine-regulated transcript (CART). Without exogenous Hh signals, mESCs initially differentiated into dorsal hypothalamic/prethalamic progenitors and finally into MCH⁺CART⁺ neurons through a specific intermediate progenitor state. Conversely, activation of the Hh pathway specified ventral hypothalamic progenitors that generate both MCH⁺CART⁻ and MCH⁺CART⁺ neurons. These results suggest that *in vivo* MCH neurons may originate from multiple cell lineages that arise through early dorsoventral patterning of the hypothalamus. Additionally, we found that Hh signaling supports the differentiation of mESCs into orexin/hypocretin neurons, a well-defined cell group intermingled with MCH neurons in the lateral hypothalamic area (LHA). The present study highlights and improves the utility of mESC culture in the analysis of the developmental programs of specific hypothalamic cell types.

Key words: 3D culture; ES cells; hypothalamus; MCH; neuronal differentiation

Significance Statement

A growing body of literature has revealed the importance of hypothalamic melanin-concentrating hormone (MCH) neurons in energy homeostasis and the cognitive function, but their developmental biology remains relatively unknown. To establish a new approach for addressing this issue, we tested the ability of an *in vitro* differentiation system of mouse embryonic stem cells (mESCs) to recapitulate the development of MCH neurons. The mESC culture robustly generated MCH-positive neurons resembling native neurons in several aspects and provided evidence that Hedgehog (Hh) signaling is a key factor to produce neurochemical subtypes of MCH neurons. Our results demonstrate the suitability of mESC culture as a platform to study the molecular mechanisms underlying the development of MCH neurons and possibly of other hypothalamic cell types.

Received October 18, 2021; accepted April 11, 2022; First published April 18, 2022.

The authors declare no competing financial interests.

Author contributions: Y.K., H.S., and H.N. designed research; Y.K., M.K., and H.N. performed research; Y.K., M.K., Y.S.K., A.N., T.K., K.S., and H.N. analyzed data; Y.K. and H.N. wrote the paper.

Introduction

Melanin-concentrating hormone (MCH) is a neuropeptide synthesized by hypothalamic neurons that project to numerous brain areas and the cerebral ventricle (Bittencourt et al., 1992; Conductier et al., 2013; Noble et al., 2018). MCH receptor 1 (MCHR1; the sole receptor in rodents) is also found widely in the CNS (Saito et al., 2001). Consistent with its brain-wide distribution, pharmacological or genetic modifications of MCH/MCHR1 signaling affect various physiological processes, particularly those related to energy homeostasis and reward (Diniz and Bittencourt, 2017). Recent evidence from opto/chemogenetics and *in vivo* calcium imaging experiments have highlighted the importance of MCH neuronal activity in regulating rapid eye movement (REM) sleep (Jego et al., 2013; Konadhode et al., 2013; Vetrivelan et al., 2016; Blanco-Centurion et al., 2019; Komagata et al., 2019), feeding behavior (Domingos et al., 2013; Noble et al., 2018; Dilsiz et al., 2020), and memory (Izawa et al., 2019; Kosse and Burdakov, 2019; Concetti et al., 2020).

Despite the growing body of literature on the physiology of MCH neurons, the number of studies focusing on their developmental process is limited. In rodents, the birth of MCH neurons occurs in mid-to-late gestation [embryonic day (E)10–E16 in rats and E9–E14 in mice] and the expression of MCH becomes evident in the prenatal period (Brischoux et al., 2001; Steininger et al., 2004; Croizier et al., 2010; Díaz et al., 2014). MCH neurons have at least two subpopulations, which are characterized by their neurochemical phenotypes, birthdates, and projection patterns (Brischoux et al., 2002; Cvetkovic et al., 2004; Croizier et al., 2010). One population co-expresses cocaine- and amphetamine-regulated transcript (CART) and neurokinin-3 receptor (NK3R), the other expresses neither of these molecules. The latter (i.e., MCH⁺CART⁻NK3R⁻ group) corresponds to initially generated MCH neurons, localized in the lateral hypothalamic area (LHA), and is the main source of descending MCH fibers to the spinal cord. The later born MCH⁺CART⁺NK3R⁺ population is distributed in the LHA and more medial hypothalamic areas and constitutes the major fraction of cortically projecting MCH neurons. The existence of these two subpopulations was recently corroborated by a single-cell transcriptomic analysis of MCH⁺ cells in the mouse LHA (Mickelsen et al., 2019). The heterogeneous nature of MCH neurons may

contribute to parallel regulation of memory processes and muscle tone during REM sleep (Hanriot et al., 2007; Hassani et al., 2009; Izawa et al., 2019). Although previous studies have identified some transcription factors and morphogens critical for MCH neuron development (Szabó et al., 2009; Sokolowski et al., 2015; Xie et al., 2017; Seifinejad et al., 2019), little is known about how the MCH neuronal subtypes are produced in the developing hypothalamus.

In vitro generation of hypothalamic neurons from embryonic stem cells (ESCs) or induced pluripotent stem cells (iPSCs) can provide insights into the specification programs of those neurons. Such a differentiation system was first established for mouse ESCs (mESCs) using three-dimensional (3D) culture named SFEBq (serum-free floating culture of embryoid body-like aggregates with quick reaggregation; Wataya et al., 2008). Since then, hypothalamic neurons have been made from human ESCs and iPSCs (hESCs/hiPSCs) in SFEBq-based 3D culture (Merkle et al., 2015; Ogawa et al., 2018; Kasai et al., 2020) or two-dimensional culture (Merkle et al., 2015; Wang et al., 2015; Rajamani et al., 2018). These hESC/hiPSC cultures would be useful for basic and clinical research on the human hypothalamus, but there are two advantages of using mESCs over hESCs/hiPSCs for general purposes: a shorter differentiation period and direct comparability with *in vivo* data from animal experiments. However, to our knowledge, no previous study has focused on MCH neuron development in mESC-based differentiation systems.

Currently, SFEBq is the only established method to efficiently induce hypothalamic differentiation of mESCs. We therefore aimed to evaluate whether this 3D culture system is suitable for analyzing the developmental process of MCH neurons. To this end, we followed the original SFEBq method and induced hypothalamic-like tissues from mESCs (ES-Hypo, hereafter). We first characterized the temporal pattern of neuronal differentiation in ES-Hypo and then traced the generation of MCH neurons in this developing tissue. We also examined the similarity of mESC-derived MCH neurons to native MCH neurons by assessing their morphologic maturation, neuronal connectivity, and neuropeptide/neurotransmitter phenotype. Finally, ES-Hypo was used to demonstrate an essential role of Hedgehog (Hh) signaling in the production of the neurochemical subtypes of MCH neurons. Our data also include data obtained from the observation of the development of orexin/hypocretin neurons, a well-defined wake-promoting cell group adjacent to MCH neurons in the LHA (Soya and Sakurai, 2020).

Materials and Methods

Cell culture

mESCs were cultured under standard conditions (37°C, 95% air, 5% CO₂) according to the original paper of ES-Hypo (Wataya et al., 2008), with some modifications. Two mESC lines, EB5 (RCB, #AES0151, RRID: CVCL_J648) and its Rax::GFP knock-in subclone (RCB, #AES0145, RRID: CVCL_J650), were maintained on gelatin-coated

This work was partially supported by Grants-in-Aid for Scientific Research (KAKENHI) from the Japan Society for the Promotion of Science (JSPS) Grant Numbers JP25505008, JP16K14556 (to H.N.), and JP20K11658 (to Y.K.), the Japan Agency for Medical Research and Development (AMED) under Grant Numbers JP20bm0404036 and JP21ek0109524 (to H.S.), and the Nitto Foundation Grant (Y.K.).

Acknowledgments: We thank Hiromi Yamazaki for technical assistance.

Y. S. Kaneko's present address: Biochemistry and Molecular Cell Biology, Faculty of Pharmacy, Gifu University of Medical Science, Kani, Gifu 509-0293, Japan.

Correspondence should be addressed to Hiroshi Nagasaki at hnagasaki@fujita-hu.ac.jp.

<https://doi.org/10.1523/ENEURO.0442-21.2022>

Copyright © 2022 Kodani et al.

This is an open-access article distributed under the terms of the Creative Commons Attribution 4.0 International license, which permits unrestricted use, distribution and reproduction in any medium provided that the original work is properly attributed.

dishes in Glasgow's minimum essential medium (Wako, #078-05525) supplemented with 1% FBS (Nichirei Biosciences, #171012), 10% knock-out serum replacement (KSR; Invitrogen, #10828028), 0.1 mM nonessential amino acids (Invitrogen, #11140050), 1 mM sodium pyruvate (Sigma, #S8636), 0.1 mM 2-mercaptoethanol (Kanto Chemical, #25099-30), 2000 U/ml leukemia inhibitory factor (Wako, #195-16053), and 20 μ g/ml blasticidin S (Wako, #029-18701). For SFEBq culture, mESCs were dissociated to single cells in 0.25% Trypsin-EDTA (Invitrogen, #25200072) and quickly reaggregated in growth factor-free chemically defined medium (gfCDM; 3000 cells/100 μ l/well) using low-cell-adhesion U-bottom 96-well plates (Sumilon PrimeSurface 96U plate, Sumitomo Bakelite). The gfCDM consisted of 1:1 Iscove's modified Dulbecco's medium (Invitrogen, #31980030)/Ham's F12 (Invitrogen, #31765035), 1% chemically defined lipid concentrate (Invitrogen, #11905031), 450 μ M monothioglycerol (Sigma, #M6145), and 5 mg/ml purified BSA (Sigma, #A9418). In some experiments (Figs. 1D, 2G,H), SFEBq culturing was performed in gfCDM supplemented with 10% KSR (gfCDM + KSR). The day on which mESCs were seeded for SFEBq culture was defined as differentiation day 0.

The original culture protocol for ES-Hypo includes fluorescence-activated cell sorting (FACS) of Rax::GFP⁺ hypothalamic progenitors on day 7 (Wataya et al., 2008). In the present study, this step was omitted because only WT mESCs were used for neuronal differentiation, except for some experiments (Fig. 7). Therefore, aggregated WT mESCs were maintained in gfCDM without any medium exchange until day 9, when 100 μ l of neuronal differentiation medium (NDM) was added per well. The NDM contained DMEM/Ham's F12 (Wako, #042-30555) supplemented with 35 mM glucose, N2 (Wako, #141-08941), MACS NeuroBrew-21 (without vitamin A; Miltenyi Biotech, #130-097-263), 10 ng/ml human CNTF (Wako, #032-18851), and penicillin/streptomycin (Wako, #168-23191). When FACS was performed on day 7, sorted Rax::GFP⁺ and GFP⁻ cells were reaggregated in DFK medium (5000 cells/100 μ l/well) using low-cell-adhesion U-bottom 96-well plates and supplied with NDM on day 10 (100 μ l/well). The DFK medium contained DMEM/Ham's F12 (Wako, #048-29785) supplemented with 10% KSR, 35 mM glucose, 10 μ M Y-27632 (Wako, #034-24024), and penicillin/streptomycin. From day 13, aggregates were cultivated at the air-liquid interface using Millicell cell culture inserts (Millipore, #MCSP06H48, RRID: SCR_015799) in NDM. Half the volume of the medium was changed every 2–3 d. In some experiments (Figs. 5, 6), Smoothened agonist (SAG; Cayman Chemical, #11914) was added to the differentiation media at 30 nM from day 4 onward.

For the dissociation culture of mESC-derived neurons, cells were dissociated from aggregates on days 19–20 or 30–33 using Neuron Dissociation Solutions (Wako, #297-78101) and plated onto poly-D-lysine/laminin-coated coverslips or 24-well plates at a density of $5.0\text{--}8.5 \times 10^4$ cells/cm² in NDM. After 3 d of adherent culture, cells were subjected to an immunocytochemical analysis or calcium imaging experiment.

Quantification of Rax::GFP⁺ cells

To examine the time-dependent change of the Rax::GFP expression, differentiating mESC aggregates (eight aggregates per day) from a single experimental batch were dissociated with Accumax (Innovative cell technologies, #AM105) to single cells, and their fluorescence images were acquired with a DMI6000B microscope (Leica MicroSystems). Rax::GFP⁺ cells were manually quantified using the cell counter plugin for Fiji (a distribution of ImageJ, RRID: SCR_002285; Schindelin et al., 2012). To verify the reproducible induction of Rax::GFP⁺ cells, their percentage was measured by flow cytometry in multiple experimental batches on day 7.

Flow cytometry and cell sorting

To measure the percentage of Rax::GFP⁺ cells on day 7, cells were dissociated from at least 32 aggregates per batch with Accumax and suspended in Cell Staining Buffer (BioLegend, #420201). Dead cells were stained with 7-AAD (Tonbo Biosciences, #13-6993), and the 7-AAD⁻ live cell fraction (>10,000 events) was analyzed using a BD FACS Calibur (BD Biosciences) and the BD CellQuest Pro software program (BD Biosciences, RRID: SCR_014489). WT mESC-derived cells were used as a negative control for setting the Rax::GFP⁺ gate.

For FACS sorting, day-7 aggregates were pretreated with 10 μ M Y-27632 for 1 h to minimize cell death during the experiment. Accumax-dissociated cells were suspended in FACS buffer consisting of HBSS(-) (Wako, #085-09355), 0.5% BSA, 1 mM EDTA, and 10 μ M Y-27632. Dead cells were stained with propidium iodide (PI; Sigma, #P4170), and Rax::GFP⁺ and GFP⁻ cells were sorted from the PI⁻ live cell fraction using MoFlo Astrios (Beckman Coulter). Sorted cells were collected in ice-cold DFK medium.

qRT-PCR

Total RNA was collected from differentiating mESC aggregates (8 aggregates per sample) using a FastPure RNA kit (TaKaRa, #9190) and converted into cDNA with Superscript II reverse transcriptase (Invitrogen, #18064022). qPCR was performed using THUNDERBIRD SYBR qPCR Mix (Toyobo, #QPS-201) and the ABI PRISM 7900HT system (Applied Biosystems). Data were normalized to the expression of the β -actin gene (*Actb*). The following primers were used: *Actb*, forward 5'-CTAAGGCCAACCGTGAA AAG-3', reverse 5'-ACCAGAGGCATACAGGGACA-3'; *Pmch*, forward 5'-CACAGGAAAAGAGAGAAATTGGG-3', reverse 5'-TGTAAGGATGTTGCGGACC-3'; *Hcrt*, forward 5'-TCTTGGGTATTTGGACCACTG-3', reverse 5'-CCCAGGGAACCTTTGTAGAAG-3'.

Calcium imaging

Dissociation cultures prepared in 24-well plates were used for calcium imaging on day 36. Before imaging, cells were subjected to a loading of the Ca²⁺ indicator Calbryte-520 AM (AAT Bioquest, #20650) and nuclear staining with Hoechst 33342 (Dojindo, #H342) as follows. 2 \times loading solution containing 10 μ M Calbryte-520 AM,

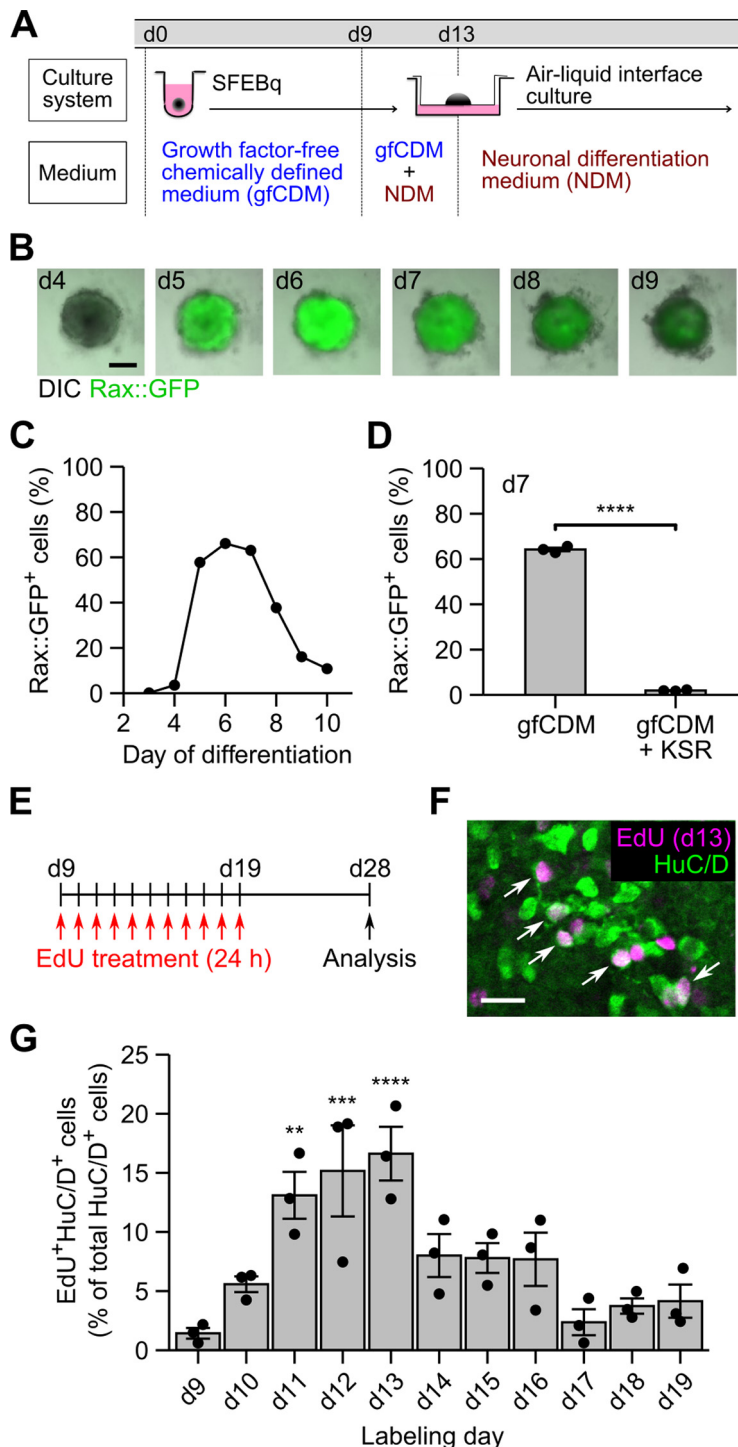


Figure 1. Temporal pattern of neuronal differentiation in ES-Hypo. **A**, Culture protocol for ES-Hypo induction. d, day. **B**, Fluorescence images of SFEBq aggregates showing the Rax::GFP expression during days 4–9. Scale bar: 200 μ m. **C**, The percentage of Rax::GFP⁺ cells during days 3–10 in a single experimental batch. **D**, The percentage of Rax::GFP⁺ cells on day 7 in multiple experimental batches ($n=3$). SFEBq culturing were performed in normal differentiation medium (gfCDM) or KSR-supplemented differentiation medium (gfCDM + KSR). **** $p < 0.0001$ by Welch’s t test. **E**, A schematic illustration of the birth-dating analysis of postmitotic neurons in ES-Hypo. **F**, A representative image of day-28 ES-Hypo stained for EdU and HuC/D. The cell aggregate was treated with EdU on day 13. Arrows indicate double-positive cells (i.e., postmitotic neurons born on day 13). Scale bar: 20 μ m. **G**, Summary of the birthdates of postmitotic neurons in ES-Hypo. The percentage of EdU⁺HuC/D⁺ cells among total HuC/D⁺ cells was quantified for each day of EdU labeling. $n=3$ aggregates per day. ** $p < 0.01$, *** $p < 0.001$, and **** $p < 0.0001$ versus day 9 by Dunnett test.

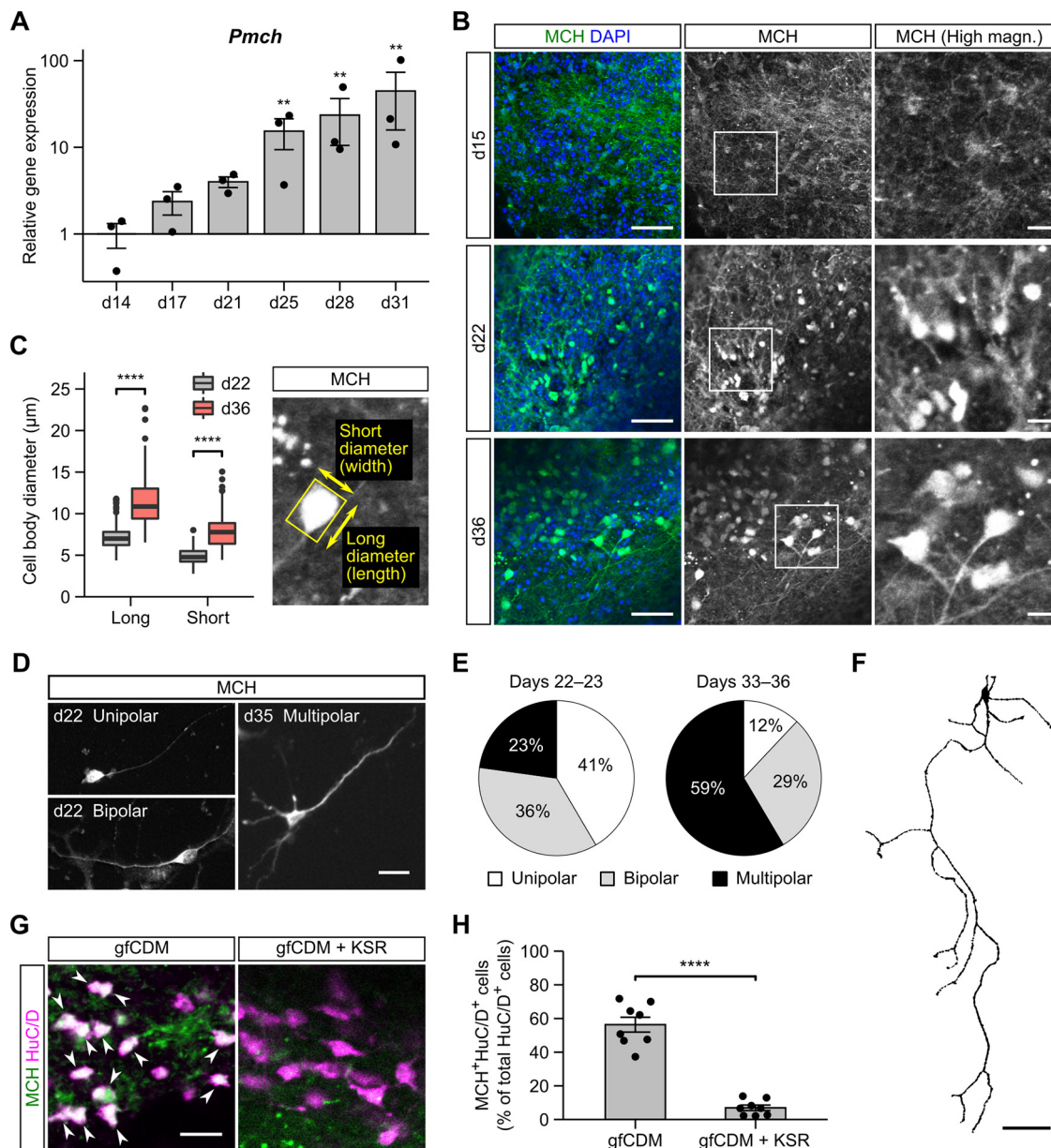


Figure 2. Generation of MCH neurons in ES-Hypo. **A**, The qRT-PCR-based analysis of the *Pmch* expression during ES-Hypo differentiation. *Pmch* encodes the precursor of MCH. Data were normalized to *Actb* and gene expression on day 14 and plotted in log10 scale. $n=3$ experiments. $**p < 0.01$ versus day 14 by Dunnett test. **B**, Immunofluorescence staining of ES-Hypo for MCH on days 15, 22, and 36. Nuclei were stained with DAPI. The right panels show high-magnification images of the boxed regions in the middle panels. Scale bars: $50\ \mu\text{m}$ (low magnification) and $10\ \mu\text{m}$ (high magnification). **C**, Quantification of the cell body diameter for MCH-ir cells on days 22 and 36. The long and short diameters for each MCH-ir cell were measured as shown in the right panel. $n=300$ cells per day. $****p < 0.0001$ by Welch's *t* test. **D–F**, The analysis of MCH-ir cells in the dissociation culture. Cells were dissociated from ES-Hypo on days 19–20 or 30–33 and cultured in a monolayer for 3 d. Representative morphologies of MCH-ir cells are shown in fluorescence images (**D**) and a cell trace (**F**). Scale bars: $20\ \mu\text{m}$ (**D**) and $50\ \mu\text{m}$ (**F**). The percentage of MCH-ir cells showing unipolar, bipolar, or multipolar morphology is presented in the pie charts (**E**) for days 22–23 ($n=272$ cells) and days 33–36 ($n=200$ cells). Functional properties of MCH-ir cells on day 36 were evaluated by calcium imaging as shown in Extended Data Figure 2-1. **G**, Representative images of day-36 mESC aggregates immunostained for MCH and HuC/D. The aggregates were initially differentiated in gfCDM (left, corresponding to ES-Hypo) or gfCDM + KSR (right). Arrowheads indicate double-positive cells. Scale bar: $20\ \mu\text{m}$. **H**, The percentage of MCH⁺HuC/D⁺ cells among total HuC/D⁺ cells under the culture conditions shown in **G**. $n=8$ aggregates per condition. $****p < 0.0001$ by Welch's *t* test.

$5\ \mu\text{g/ml}$ Hoechst 33342, and 0.04% Pluronic F-127 (Biotium, #59004) was prepared in artificial CSF (ACSF). The composition of ACSF was (in mM) $132\ \text{NaCl}$, $3\ \text{KCl}$, $1.3\ \text{MgCl}_2$, $2.4\ \text{CaCl}_2$, $20\ \text{NaHCO}_3$, $1.2\ \text{KH}_2\text{PO}_4$, $3\ \text{HEPES}$,

and $10\ \text{glucose}$. Half the volume of the culture medium was changed with $2\times$ loading solution, and cells were cultured for $60\text{--}90\ \text{min}$. Cells were then washed and maintained in ACSF at room temperature (RT) before and

Table 1: Primary and secondary antibodies used for immunofluorescence staining

	Host	Dilution	Source; catalog number	RRID
Primary antibody				
HuC/D	Mouse	1 μ g/ml	Thermo Fisher Scientific; A-21271	AB_221448
MCH	Rabbit	1:3000	Phoenix Pharmaceuticals; H-070-47	AB_10013632
Orexin-A	Goat	1:250	Santa Cruz Biotechnology; sc-8070	AB_653610
GAD67	Mouse	1:500	Millipore; MAB5406	AB_2278725
VGLUT2	Guinea pig	1:500	Millipore; AB2251-I	AB_2665454
Nesfatin-1	Sheep	2 μ g/ml	R&D Systems; AF6895	AB_10972964
CART	Chicken	1:500	Millipore; AB5340P	AB_91795
Rax	Guinea pig	1:2000	TaKaRa; M229	AB_2783559
Pax6	Mouse	1:100	DSHB; PAX6	AB_528427
Nkx2.1	Rabbit	1:200	Santa Cruz Biotechnology; sc-13040	AB_793532
Nkx2.1	Mouse	1:500	MBL; K0121-3	AB_592930
Sox1	Goat	1:500	R&D Systems; AF3369	AB_2239879
Foxg1	Rabbit	1:1000	TaKaRa; M227	AB_2827749
Nkx2.2	Mouse	1:50	DSHB; 74.5A5	AB_531794
NK3R	Rabbit	1:1000	Novus Biologicals; NB300-102SS	AB_2287128
GFP	Chicken	1:500	Thermo Fisher Scientific; A10262	AB_2534023
Secondary antibody				
Anti-mouse, Alexa Fluor 488	Goat	1:1000	Thermo Fisher Scientific; A-11029	AB_2534088
Anti-rabbit, Alexa Fluor 488	Donkey	1:1000	Thermo Fisher Scientific; A-21206	AB_2535792
Anti-chicken, Alexa Fluor 488	Donkey	1:500	Jackson ImmunoResearch; 703-545-155	AB_2340375
Anti-goat, Alexa Fluor 488	Donkey	1:1000	Thermo Fisher Scientific; A-11055	AB_2534102
Anti-mouse, Alexa Fluor 555	Donkey	1:1000	Thermo Fisher Scientific; A-31570	AB_2536180
Anti-rabbit, Alexa Fluor 555	Donkey	1:1000	Thermo Fisher Scientific; A-31572	AB_162543
Anti-goat, Alexa Fluor 555	Donkey	1:1000	Thermo Fisher Scientific; A-21432	AB_2535853
Anti-sheep, Alexa Fluor 555	Donkey	1:1000	Thermo Fisher Scientific; A-21436	AB_2535857
Anti-mouse, Alexa Fluor 594	Donkey	1:1000	Thermo Fisher Scientific; A-21203	AB_141633
Anti-rabbit, Alexa Fluor 594	Donkey	1:1000	Thermo Fisher Scientific; A-21207	AB_141637
Anti-guinea pig, Cy3	Donkey	1:500	Jackson ImmunoResearch; 706-165-148	AB_2340460
Anti-mouse, Alexa Fluor 647	Donkey	1:1000	Thermo Fisher Scientific; A-31571	AB_162542
Anti-rabbit, Alexa Fluor 647	Donkey	1:1000	Thermo Fisher Scientific; A-31573	AB_2536183

during imaging. To measure Ca^{2+} responses, time-lapse images of cells were captured at six time points (0, 60, 120, 250, 310, and 370 s) using the Opera Phenix high-content imaging system (PerkinElmer). Cells were stimulated with KCl, glutamate, or GABA at 210 s. For KCl stimulation, extracellular fluid (ECF) was manually changed from ACSF to high- K^+ ACSF containing 50 mM KCl and 85 mM NaCl. Glutamate and GABA were applied by replacing half the volume of ECF with ACSF containing 200 μ M glutamate or GABA. After calcium imaging, cells were fixed with 4% PFA in PBS for 10 min and subjected to immunocytochemistry for MCH to identify MCH-expressing cells. Calbryte-520 fluorescence from the identified MCH⁺ cells was quantified using the Harmony software program (PerkinElmer) by measuring mean pixel intensity in somatic areas, which were automatically detected based on nuclear staining with Hoechst. The fluorescence intensity was graphed as $\Delta F/F_0$, where ΔF is the intensity difference compared with background fluorescence (F_0). The intensity value at 120 s was used as F_0 . Responding cells were defined as the cells with $\Delta F/F_0 > 0.5$ at 370 s because spontaneous fluctuations in $\Delta F/F_0$ were limited in ± 0.5 .

Immunofluorescence staining

After more than two weeks of differentiation, mESC aggregates were analyzed by whole-mount immunohistochemistry as follows. First, aggregates were fixed with 4% PFA in PBS for 20 min at RT. Fixed aggregates were blocked and

permeabilized with 5% normal donkey serum (NDS) and 0.5% Triton X-100 in PBS for 1 h at RT and then incubated with primary antibodies overnight at 4°C, except that incubation with an anti-orexin-A antibody was performed for 36–48 h. After washing in PBS supplemented with 0.05% Triton X-100 (PBSX), aggregates were incubated with appropriate secondary antibodies for 1 h at RT. In this step, nuclear staining with DAPI (Dojindo, #D523) was performed simultaneously. Antibodies and DAPI were diluted with PBS containing 5% NDS and 0.1% Triton X-100 just before use. Finally, aggregates were washed in PBSX and mounted on glass slides using Fluoromount (Diagnostic BioSystems, #K024). The antibodies used in this study are listed in Table 1.

For the immunohistochemical analysis of aggregates cultured for 7–13 d, they were fixed with 4% PFA for 1 h at RT and cryoprotected in sucrose solutions of increasing concentrations (10, 20, and 30%) for 30 min each, followed by embedding in O.C.T. compound (Sakura, #4583). Serial 10- μ m-thick cryosections were prepared with a CM3050S cryostat (Leica Biosystems) and mounted on PLATINUM PRO adhesive slides (Matsunami, #SPRO-02). The sections were blocked and permeabilized with 5% NDS and 0.1% Triton X-100 in PBS for 30 min at RT and then immunostained as described above.

For the immunocytochemical analysis of dissociation cultures, cells were fixed with 4% PFA for 10 min at RT and then processed in the same way as cryosections.

Fluorescence images of whole-mount aggregates were obtained using a LSM710 confocal microscope (Carl Zeiss), and those of cryosections and dissociation cultures were obtained using a DMI6000B microscope, LSM710 confocal microscope, or BZ-9000 microscope (Keyence).

Birth-dating analysis of postmitotic neurons

During days 9–19, mESC aggregates were cultured for 24 h in the differentiation medium containing 10 μM 5-ethynyl-2'-deoxyuridine (EdU) by the day. After the EdU treatment, aggregates were washed and cultured in differentiation medium free of EdU until day 28 and fixed with 4% PFA for 20 min at RT. Aggregates were then subjected to visualization of EdU, followed by immunofluorescence staining for the neuronal marker HuC/D. The EdU labeling and staining were performed using a Click-iT EdU Alexa Fluor 647 Imaging kit (Invitrogen, #C10340). Fluorescence images were captured with a LSM710 confocal microscope, and EdU⁺HuC/D⁺ double-positive cells were considered to be postmitotic neurons born during EdU treatment. Cell counts were performed as described below.

The imaging analysis of immunofluorescence data

The long and short diameters of MCH⁺ cell bodies were measured using the straight line and measure tools in Fiji. In the birth-dating analysis of postmitotic neurons, the percentage of EdU⁺ cells in the HuC/D⁺ neuronal population was determined as follows. First, in the fluorescence images acquired from each aggregate, HuC/D⁺ cells were manually quantified using the cell counter plugin for Fiji (200–500 positive cells per aggregate). Next, EdU⁺ cells were counted in the prequantified HuC/D⁺ population to calculate the percentage of its EdU⁺ fraction. Although a part of HuC/D⁺ cells exhibited diffuse EdU staining, they were also considered as EdU⁺ cells. This analysis protocol was also applied to determine the MCH⁺ percentage in the HuC/D⁺ population, the HuC/D⁺ percentage in the MCH⁺ population, and the positive rates of neurochemical markers in the MCH⁺ population. For the analysis of cryosections, fluorescence images were acquired from three non-adjacent sections per aggregate. Several images from day-7 aggregates were analyzed using the Columbus software program (PerkinElmer) to calculate the Pax6⁺ or Nkx2.1⁺ percentage in the Rax⁺ cell population semi-automatically (200–400 Rax⁺ cells were detected per aggregate).

Statistical analysis

Statistical analyses were performed using the R software program (version 4.0.5, The R Foundation, RRID: SCR_001905). Results of grouped data were presented as the mean \pm SEM in the text or figures (bar plots). Some data were presented with box plots showing the median (bold line), interquartile range (IQR; box), and ± 1.5 IQR (whisker) with outliers (Fig. 2C) or all data points (Fig. 5H). Statistical significance between two groups was assessed by Welch's *t* test, except for Figure 5H, in which

two groups were compared using the Brunner–Munzel test, which does not require assumptions of normality and homoscedasticity. For time series data, statistical significance between the earliest time point and other time-points was assessed by Dunnett test. For statistical analysis of qRT-PCR data, a log₁₀ transformation was performed to reduce variability of data. The results of the statistical analyses are summarized in Table 2.

Results

ES-Hypo recapitulates the temporal pattern of hypothalamic development

The SFEBq method, using gfCDM, efficiently induces Rax⁺ hypothalamic progenitors from mESCs after 7 d of differentiation (Wataya et al., 2008). Rax is a transcription factor specifically expressed in the hypothalamic and retinal neuroepithelium (Furukawa et al., 1997; Mathers et al., 1997; Shimogori et al., 2010; Lu et al., 2013). The Rax⁺ progenitors subsequently generate their neuronal derivatives, such as vasopressin cells, after 20 or more days (Wataya et al., 2008). In this culture system, however, the time course of neuronal differentiation has not been fully characterized. We therefore started our study by systematically tracing Rax⁺ cell induction and subsequent neurogenesis during ES-Hypo development (Fig. 1A).

To monitor Rax⁺ cell generation in real time, a Rax::GFP reporter mESC line (Wataya et al., 2008) was subjected to SFEBq culture. The expression of Rax::GFP was sharply increased on day 5 and was maintained until day 7 in a large proportion of aggregated cells, followed by a gradual decrease (Fig. 1B,C). A flow cytometric analysis on day 7 confirmed that Rax::GFP⁺ progenitors were reproducibly induced in gfCDM (~64% of total cells) but greatly decreased when the medium was supplemented with KSR (~2% of total cells; Fig. 1D). KSR is a widely used serum replacement with minimal growth factors, but it is reported to severely inhibit hypothalamic differentiation of mESCs via activating the insulin/PI3K/Akt pathway and rather induce telencephalic differentiation (Wataya et al., 2008). Since the expression of Rax::GFP was downregulated from days 7–10 (Fig. 1C), we expected that neurogenesis starts in this period. To evaluate the time course of neurogenesis, we conducted a birth-dating analysis using the thymidine analog EdU during days 9–19. Newly born postmitotic neurons were labeled with EdU by the day, and they were quantified on day 28 as EdU and HuC/D (a neuronal marker) double-positive cells (Fig. 1E,F). The results of the analysis were summarized in Figure 1G. The birth of postmitotic neurons has already occurred on day 9, and it reached a peak during days 11–13 (roughly half of HuC/D⁺ neurons were born in this period) and persisted at lower levels thereafter. Eventually, 85% of HuC/D⁺ neurons were generated throughout the labeling period. Taken together, hypothalamic progenitor specification occurs within the first week of mESC differentiation and after neurogenesis, mostly within the second and third weeks. Considering that mESCs are derived from blastocysts (~E3.5 embryos), this time course resembles the temporal pattern of embryonic development of the

Table 2: Statistical table

Figure	Group comparison	Data structure	Type of test	<i>p</i> value	95% confidence interval
1D	gfCDM vs gfCDM + KSR	Normal distribution	Welch's <i>t</i> test	<i>p</i> < 0.0001	59.03, 65.52
1G	d9 vs d10	Normal distribution	Dunnett test	<i>p</i> = 0.55798	−3.63, 11.94
	d9 vs d11	Normal distribution	Dunnett test	<i>p</i> = 0.00166	3.89, 19.46
	d9 vs d12	Normal distribution	Dunnett test	<i>p</i> = 0.00033	5.95, 21.52
	d9 vs d13	Normal distribution	Dunnett test	<i>p</i> < 0.0001	7.41, 22.98
	d9 vs d14	Normal distribution	Dunnett test	<i>p</i> = 0.12627	−1.21, 14.37
	d9 vs d15	Normal distribution	Dunnett test	<i>p</i> = 0.14666	−1.42, 14.16
	d9 vs d16	Normal distribution	Dunnett test	<i>p</i> = 0.15859	−1.53, 14.05
	d9 vs d17	Normal distribution	Dunnett test	<i>p</i> = 0.99996	−6.85, 8.73
	d9 vs d18	Normal distribution	Dunnett test	<i>p</i> = 0.95885	−5.48, 10.09
	d9 vs d19	Normal distribution	Dunnett test	<i>p</i> = 0.90193	−5.06, 10.51
2A*	d14 vs d17	Normal distribution	Dunnett test	<i>p</i> = 0.5707	−0.20, 1.51
	d14 vs d21	Normal distribution	Dunnett test	<i>p</i> = 0.1578	−5.06, 10.51
	d14 vs d25	Normal distribution	Dunnett test	<i>p</i> = 0.0093	0.28, 1.99
	d14 vs d28	Normal distribution	Dunnett test	<i>p</i> = 0.0036	0.45, 2.16
	d14 vs d31	Normal distribution	Dunnett test	<i>p</i> = 0.0010	0.66, 2.38
2C, "long"	d22 vs d36	Normal distribution	Welch's <i>t</i> test	<i>p</i> < 0.0001	−4.53, −3.86
2C, "short"	d22 vs d36	Normal distribution	Welch's <i>t</i> test	<i>p</i> < 0.0001	−3.15, −2.69
2H	gfCDM vs gfCDM + KSR	Normal distribution	Welch's <i>t</i> test	<i>p</i> < 0.0001	38.75, 60.04
3B*	d14 vs d31	Normal distribution	Welch's <i>t</i> test	<i>p</i> = 0.01818	−2.89, −0.52
5C, top	SAG (−) vs (+)	Normal distribution	Welch's <i>t</i> test	<i>p</i> < 0.0001	70.25, 93.41
5C, bottom	SAG (−) vs (+)	Normal distribution	Welch's <i>t</i> test	<i>p</i> < 0.0001	−92.79, −82.23
5F	SAG (−) vs (+)	Normal distribution	Welch's <i>t</i> test	<i>p</i> = 0.009963	−45.36, −8.52
5H	SAG (−) vs (+)	Normality not assumed	Brunner–Munzel test	<i>p</i> < 0.0001	0.77, 1.04

*Log10-transformed data were used for statistical analysis.

mouse hypothalamus (Shimada and Nakamura, 1973; Ishii and Bouret, 2012; Lu et al., 2013).

Development of MCH neurons in ES-Hypo

Based on the determined time course of neurogenesis, we explored MCH neuron development in ES-Hypo after two weeks of differentiation. qRT-PCR showed that MCH mRNA levels increased exponentially during weeks 3–5 (Fig. 2A). MCH-immunoreactivity was faintly observed on day 15, but clear MCH-immunoreactive (ir) cell bodies and fibers appeared on day 22 (Fig. 2B). These MCH-ir cell bodies were characterized by round shapes and small diameters (<10 μm), both of which are features of immature MCH neurons (Steininger et al., 2004; Li et al., 2018). After 36 d of culture, MCH-ir cells were often angular-shaped and larger in comparison to MCH-ir cells on day 22 (Fig. 2B,C), which is reminiscent of neuronal maturation *in vivo* (Steininger et al., 2004; Li et al., 2018). Another hallmark of neuronal maturation is neurite growth; while young MCH neurons have only one or two neurites (i.e., unipolar or bipolar cells), a major fraction of adult MCH neurons are multipolar cells with an axon and 2–5 primary dendrites (Steininger et al., 2004; Diniz et al., 2019). To assess morphologic changes in mESC-derived MCH⁺ cells in terms of neurite number, we prepared dissociation cultures from ES-Hypo on different days. Immunocytochemistry showed that 77% of MCH-ir cells were classified into unipolar or bipolar cells on days 22–23, but 59% of MCH-ir cells exhibited a multipolar morphology on days 33–36 (Fig. 2D,E). Some of the multipolar cells displayed an extended and branched axonal process (Fig. 2F). We also performed a calcium imaging experiment in the dissociation culture

on day 36 and found that most MCH-ir cells were activated by KCl or glutamate but not by GABA (Extended Data Fig. 2-1). These morphologic and functional properties strongly support the neuronal identity of MCH-ir cells, and we further confirmed that the neuronal marker HuC/D was expressed in 93.2 ± 1.2% of MCH-ir cells (*n* = 8 aggregates on day 36; Fig. 2G, left). The MCH⁺ percentage of total HuC/D⁺ neurons varied among individual aggregates (37–72%) but became much lower (2–13%) when SFEBq culturing had been performed in KSR-containing medium (Fig. 2G,H). These data indicate that ES-Hypo robustly generates MCH neurons, which reproduce the morphologic development of native MCH neurons.

Putative synaptic connections between MCH and orexin neurons in ES-Hypo

The axon growth observed for MCH neurons in ES-Hypo suggests that they may form synaptic connections with other differentiated neurons. There is some histologic and electrophysiological evidence to support reciprocal connections between MCH neurons and neighboring orexin neurons in the LHA (Bayer et al., 2002; Guan et al., 2002; van den Pol et al., 2004; Tortorolo et al., 2006; Rao et al., 2008; Apergis-Schoute et al., 2015), which may be implicated in sleep/wake control (Konadhode et al., 2014; Hung et al., 2020). To test the possibility that such local wiring occurs in ES-Hypo, we first analyzed the differentiation of orexin neurons. Although orexin-ir cells were rarely observed before day 25, we encountered clusters of orexin-ir cells, showing neuronal morphologies, in a fraction of mESC aggregates cultured for four to five weeks (~25% of the aggregates tested; Fig. 3A).

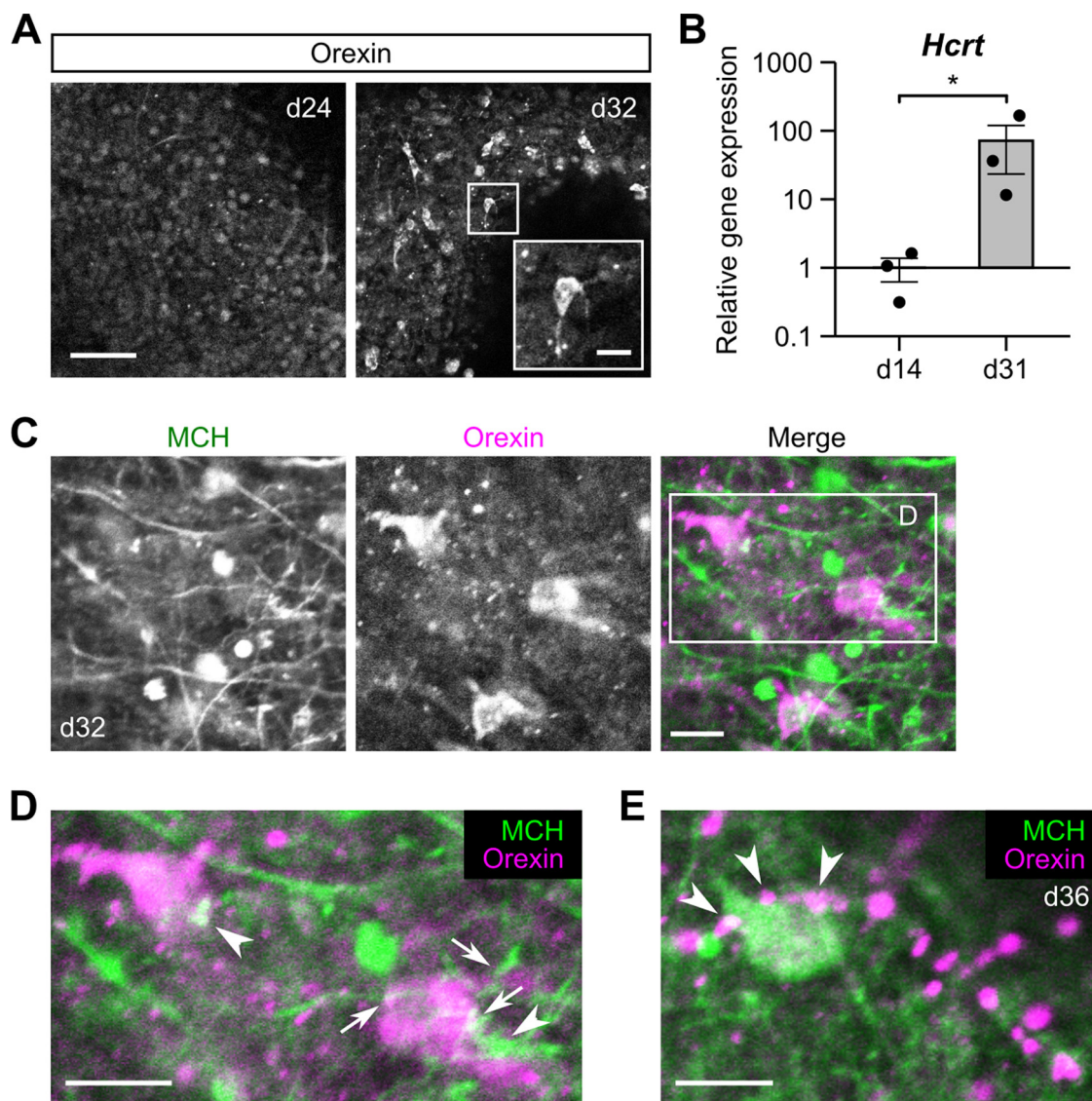


Figure 3. Reciprocal connectivity between MCH and orexin neurons in ES-Hypo. **A**, Representative images of ES-Hypo immunostained for orexin on days 24 and 32. The inset shows a magnified view of an orexin-ir cell in the boxed region. Scale bars: 50 and 10 μm (inset). **B**, The qRT-PCR-based analysis of the *Hcrt* expression on days 14 and 31. *Hcrt* encodes the precursor of orexin. Data were normalized to *Actb* and gene expression on day 14 and plotted in log10 scale. $n = 3$ experiments. $*p < 0.05$ by Welch's *t* test. **C–E**, Double-immunofluorescence images showing putative connections between MCH-ir and orexin-ir cells in ES-Hypo on days 32 and 36. The boxed region in **C** is magnified in **D**. Two orexin-ir cells are contacted by MCH-ir fibers (**D**, arrows) or boutons (**D**, arrowheads). Similarly, an MCH-ir cell is closely apposed by orexin-ir boutons (**E**, arrowheads). Scale bars: 10 μm .

Consistent with this immunoreactivity, orexin mRNA levels were significantly higher on day 31 than on day 14 (Fig. 3B). Based on these results, we next performed double immunofluorescence staining for MCH and orexin in ES-Hypo cultured for more than one month. Confocal microscopy of orexin-rich aggregates showed that orexin-ir cells were largely immunonegative for MCH and $<10\%$ of them were detected as double-positive cells (Fig. 3C). However, single-positive orexin-ir perikarya were often apposed by MCH-ir fibers or boutons (Fig. 3D). Similarly, we identified MCH-ir cells in contact with orexin-ir boutons (Fig. 3E). These findings support the hypothesis that ES-Hypo

can produce some MCH-orexin neuronal networks that possibly resemble those in the LHA.

Neuropeptide/neurotransmitter phenotype of MCH neurons in ES-Hypo

MCH neurons are known to express other neuropeptides, including CART and nesfatin-1, and GABAergic/glutamatergic markers such as GAD67 (a GABA-synthesizing enzyme) and VGLUT2 (a machinery for glutamate uptake into synaptic vesicles; Broberger, 1999; Vrang et al., 1999; Brailoiu et al., 2007; Sapin et al., 2010; Chee et al., 2015; Mickelsen et al., 2017). To

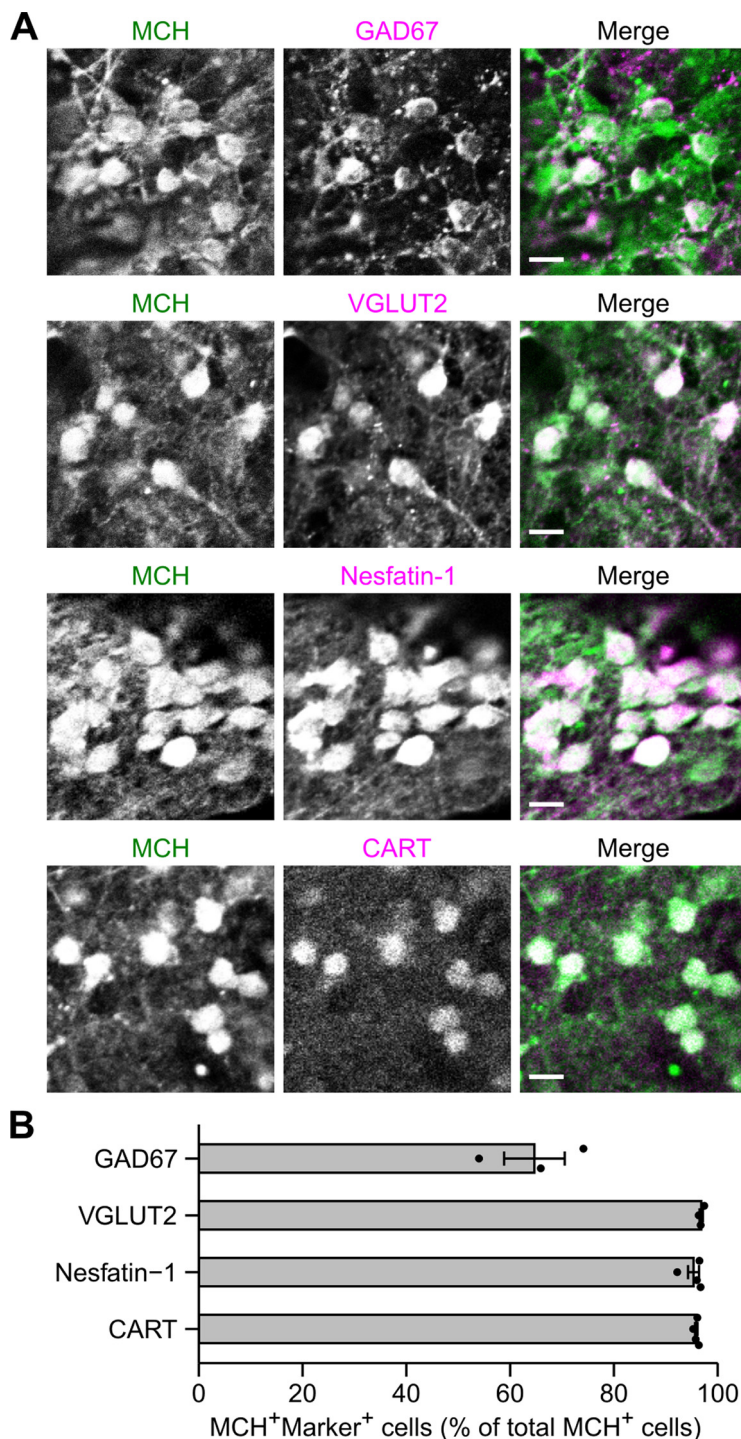


Figure 4. Characterization of neuropeptide/neurotransmitter phenotype of MCH neurons in ES-Hypo. **A**, Representative images of day-36 ES-Hypo immunostained for MCH and different neurochemical markers GAD67, VGLUT2, nesfatin-1, and CART. Scale bars: 10 μ m. **B**, The percentage of MCH⁺ cells expressing different neurochemical markers. $n = 3$ –4 aggregates per marker.

examine whether mESC-derived MCH neurons have a similar neurochemical profile, we performed double immunofluorescence staining for MCH and the above markers in ES-Hypo on day 36 (Fig. 4A). Nesfatin-1 and VGLUT2 were expressed in 95.3% and 96.8% of MCH neurons in ES-Hypo, respectively (Fig. 4B), which is comparable to the values for MCH neurons *in vivo* (Fou

et al., 2008; Fort et al., 2008; Vas et al., 2013; Chee et al., 2015; Mickelsen et al., 2017; Schneeberger et al., 2018; Naganuma et al., 2019; Hung et al., 2020). The expression of GAD67 was previously detected in 85% of native MCH neurons by an *in situ* hybridization (ISH) analysis (Sapin et al., 2010; Jego et al., 2013; Mickelsen et al., 2017), but the GAD67-ir fraction of MCH neurons

in ES-Hypo was somewhat smaller (64.7%; Fig. 4B). Because immunostaining methods are less sensitive than ISH in the detection of cell bodies of neurons that express low levels of GAD mRNAs (Esclapez et al., 1994), it is likely that the GAD67⁺ ratio of mESC-derived MCH neurons is similar to that of native MCH neurons. In contrast, this similarity in the population ratio was not observed for CART; while MCH⁺CART⁺ neurons constitute only half of the whole MCH⁺ population in the mouse hypothalamus (Croizier et al., 2010; Mickelsen et al., 2017), 95.9% of MCH-ir cells in ES-Hypo were labeled by an anti-CART antibody (Fig. 4B). Collectively, mESC-derived MCH neurons share a series of neuropeptide/neurotransmitter markers with native MCH neurons and mostly represent the CART⁺ subpopulation.

Hh signaling is critical for generating CART-negative MCH neurons and orexin neurons from mESCs

In the above-mentioned experiments (Figs. 1-4), SFEBq culturing was performed without exogenous morphogenic factors. This condition is reported to induce dorsal hypothalamic progenitors (Rax⁺Pax6⁺; Fig. 5A), whereas the addition of Shh, an endogenous Hh pathway agonist, can generate ventral hypothalamic progenitors (Rax⁺Nkx2.1⁺; Fig. 5A; Wataya et al., 2008). To examine whether Hh signaling affects mESC differentiation into CART-negative MCH neurons, we used SAG, a small-molecule agonist of the Hh pathway. In the absence of SAG, induced Rax⁺ progenitors were largely positive for the dorsal hypothalamic marker Pax6 but only partially positive for the ventral hypothalamic marker Nkx2.1 (Fig. 5B,C), as reported previously (Wataya et al., 2008). Treatment with SAG from day 4 did not greatly alter the Rax::GFP⁺ percentage on day 7 (49.3 ± 0.1%, *n* = 3 experiments) but dramatically increased the Rax⁺Nkx2.1⁺ population at the cost of the Rax⁺Pax6⁺ population (Fig. 5B,C). The SAG treatment did not affect the efficiency of neural differentiation, as indicated by the expression of the general neural progenitor marker Sox1 (Extended Data Fig. 5-1). We also found that not only Rax⁺ but also Rax⁻ cells largely expressed Nkx2.1 in the SAG-treated aggregates (Fig. 5B). Although Nkx2.1 can be expressed in telencephalic progenitors (Shimamura et al., 1995; Marín et al., 2002; Fig. 5A), the pan-telencephalic marker Foxg1 was almost absent in the SAG-treated aggregates (Fig. 5D), suggesting that the Rax⁻Nkx2.1⁺ cells are of hypothalamic lineage. In the early hypothalamic neuroepithelium, the Rax⁻Nkx2.1⁺ territories are located anterior and posterior to the Rax⁺Nkx2.1⁺ tuberal subregion and partly overlap with a longitudinal band expressing the transcription factor Nkx2.2 (Shimamura et al., 1995; Shimogori et al., 2010; Lu et al., 2013; Díaz et al., 2014; Ferran et al., 2015; Fig. 5A). We confirmed that the Rax⁻Nkx2.1⁺ portions of the SAG-treated aggregates significantly overlapped with the Nkx2.2⁺ portions (Fig. 5D). These data indicate that the SAG treatment specifies Nkx2.1⁺ ventral hypothalamic progenitors, which comprise heterogeneous subpopulations.

Subsequent culture with the continuous addition of SAG still produced many MCH-ir neurons (Extended Data Fig. 5-2), but they contained a larger proportion of CART-negative cells in comparison to MCH neurons without SAG (Fig. 5F). MCH⁺CART⁻ neurons were generally found in clusters and not co-distributed with MCH⁺CART⁺ neurons (Fig. 5E), implying separate developmental pathways for both populations. Since CART⁺ but not CART⁻ MCH neurons specifically express NK3R *in vivo* (Croizier et al., 2010), we further tested NK3R-immunoreactivity in SAG-treated samples. Because the expression of CART was limited to the MCH⁺ cell population (Fig. 5E, left), we simply performed double immunostaining for CART/NK3R and found over 95% co-localization of these markers (Extended Data Fig. 5-3). This result indicates that NK3R is expressed in the MCH⁺CART⁺ but not MCH⁺CART⁻ cell group in ES-Hypo, as in the native hypothalamus. The SAG treatment also influenced the differentiation of orexin neurons. Orexin-ir cells were nearly absent in SAG-free ES-Hypo on day 30, but several orexin-ir cells were found in the majority of SAG-treated ES-Hypo on the same day (Fig. 5G,H). Together, our findings suggest that the activation of the Hh pathway is necessary for the differentiation of mESCs into certain types of LHA cells, including CART-negative MCH neurons and orexin neurons, and that such LHA cells are derived from ventral hypothalamic progenitors.

Since both CART⁺ and CART⁻ MCH neurons as well as orexin neurons were simultaneously produced in SAG-treated ES-Hypo, we reevaluated whether the MCH-orexin neuronal connectivity is specific to either subtype of MCH neurons. We performed triple immunostaining for MCH/orexin/CART but could not determine which subtypes of MCH neurons send fibers to orexin neurons, because CART-immunoreactivity was weak or undetectable in the fiber compartment (Fig. 5E). On the other hand, we observed both MCH⁺CART⁺ and MCH⁺CART⁻ cell bodies in contact with orexin-ir boutons (Fig. 5I). Thus, both subtypes of MCH neurons seem to receive orexinergic inputs in ES-Hypo.

Progenitor origin of MCH neurons in ES-Hypo

Our results suggest that MCH neurons develop from multiple progenitor lineages which are specified through early dorsoventral patterning of the hypothalamus. To better understand the differentiation process of MCH neurons, we examined the expression patterns of regional markers as well as differentiation markers in ES-Hypo from days 7–22.

We first focused on SAG-treated ES-Hypo. On day 7, differentiating mESCs were mostly in the Nkx2.1⁺Sox1⁺ progenitor state and only partially positive for the neuronal marker HuC/D (Fig. 6A). On day 13, the robust expression of Nkx2.1 was still maintained, but there was a significant increase in HuC/D⁺ neurons, associated with downregulation of Sox1 (Fig. 6A,C,D). Most of the HuC/D⁺ neurons expressed Nkx2.1 (Fig. 6C), confirming that Nkx2.1⁺ progenitors are the primary source of postmitotic neurons in the presence of SAG. Indeed, we often observed Nkx2.1⁺Sox1⁺ rosette structures surrounded by HuC/D⁺ neurons (Fig. 6F,G), probably representing active sites of

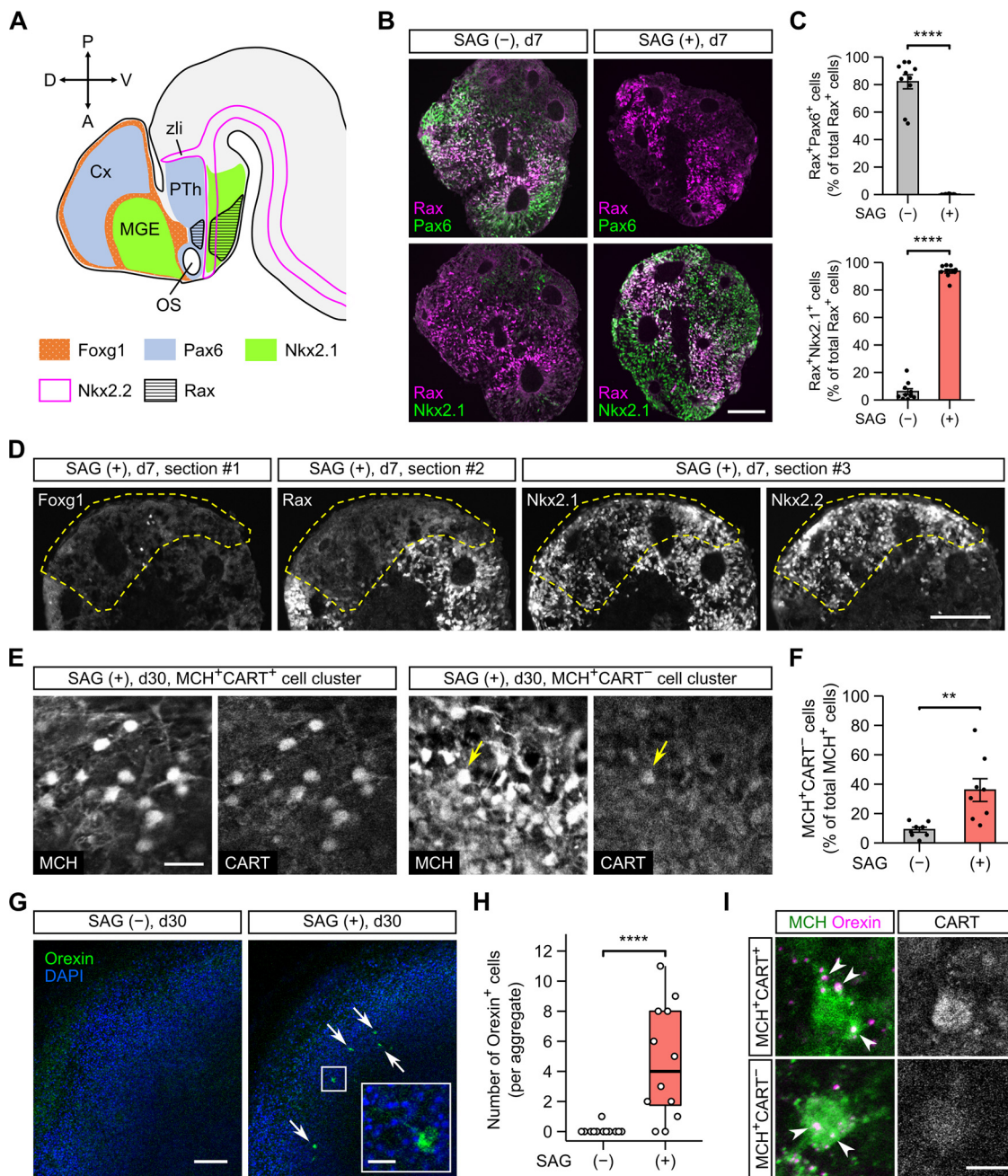


Figure 5. The generation of CART-negative MCH neurons and orexin neurons is increased by the activation of Hh signaling in ES-Hypo. **A**, The regional expression of transcription factors in the telencephalon and anterior diencephalon of embryonic mouse brain around E12. The indicated expression patterns are based on the published literature (Shimamura et al., 1995; Marin et al., 2002; Shimogori et al., 2010; Lu et al., 2013; Díaz et al., 2014; Ferran et al., 2015). Cx, cortex; MGE, medial ganglionic eminence; OS, optic stalk; PTh, prethalamus; zli, zona limitans intrathalamica. **B**, Representative images of day-7 mESC aggregates immunostained for Rax and Pax6 (upper panels) or Nkx2.1 (lower panels). The aggregates were differentiated in the absence (-) or presence (+) of 30 nM SAG. Scale bar: 100 μ m. Immunostaining for the general neural progenitor marker Sox1 is presented in Extended Data Figure 5-1. **C**, The percentage of Rax⁺ cells expressing Pax6 (top) or Nkx2.1 (bottom) on day 7 under SAG (-) and (+) conditions. $n = 10$ aggregates per condition. **** $p < 0.0001$ by Welch's t test. **D**, Serial sections from a day-7 aggregate cultured with SAG. The sections were stained for Foxg1 (#1), Rax (#2), or Nkx2.1/Nkx2.2 (#3). A Rax⁻ region is surrounded by dashed lines. Scale bar: 100 μ m. **E**, Representative immunofluorescence images of MCH⁺CART⁺ (left) and MCH⁺CART⁻ (right) cell clusters in SAG-treated aggregates on day 30. In the MCH⁺CART⁻ cluster, only one MCH⁺ cell is weakly stained for CART (arrow). Scale bar: 20 μ m. In Extended Data Figure 5-2, we assessed the co-expression of MCH and HuC/D in SAG-treated aggregates. In Extended Data Figure 5-3, we assessed the co-expression of CART and NK3R in SAG-treated aggregates. **F**, The percentage of MCH⁺CART⁻ cells among total MCH⁺ cells on day 30 under SAG (-) and (+) conditions. $n = 8$ aggregates per condition. ** $p < 0.01$ by Welch's t test. **G**, Representative images of SAG-treated (right) and untreated (left) aggregates immunostained for orexin on day 30. Arrows

continued

indicate orexin-ir cells. The inset shows a magnified view of an orexin-ir cell in the boxed region. Scale bars: 100 and 20 μm (inset). **H**, Quantification of orexin⁺ cells on day 30 under SAG (-) and (+) conditions. $n = 12$ aggregates per condition. **** $p < 0.0001$ by Brunner–Munzel test. **I**, Representative images of an MCH⁺CART⁺ (top) or MCH⁺CART⁻ (bottom) cell, which is contacted by orexin-ir boutons (arrowheads). Triple immunostaining was performed in SAG-treated aggregates on day 36. Scale bar: 10 μm .

neurogenesis. The expression of Pax6 was completely absent on day 13 (data not shown), as on day 7 (Fig. 5B). The expression of Nkx2.2 was sustained from days 7–13 (Fig. 6A) and confined to roughly half of Nkx2.1⁺ cells, including HuC/D⁺ neurons (Fig. 6B) and Sox1⁺ rosette cells (Fig. 6E). Thus, two subtypes of Nkx2.1⁺ progenitors, Nkx2.1⁺Nkx2.2⁺ and Nkx2.1⁺Nkx2.2⁻, both undergo

neurogenesis. On day 22, Nkx2.1 and Nkx2.2 were expressed in 40% and 30% of MCH-ir cells, respectively (Fig. 6H,I). We wondered whether the expression of Nkx2.2 is specific to either CART⁺ or CART⁻ MCH neurons, but Nkx2.2-immunoreactivity was clearly detected in both subtypes of MCH neurons (Fig. 6J). These results indicate that Nkx2.1⁺Nkx2.2⁺ progenitors directly

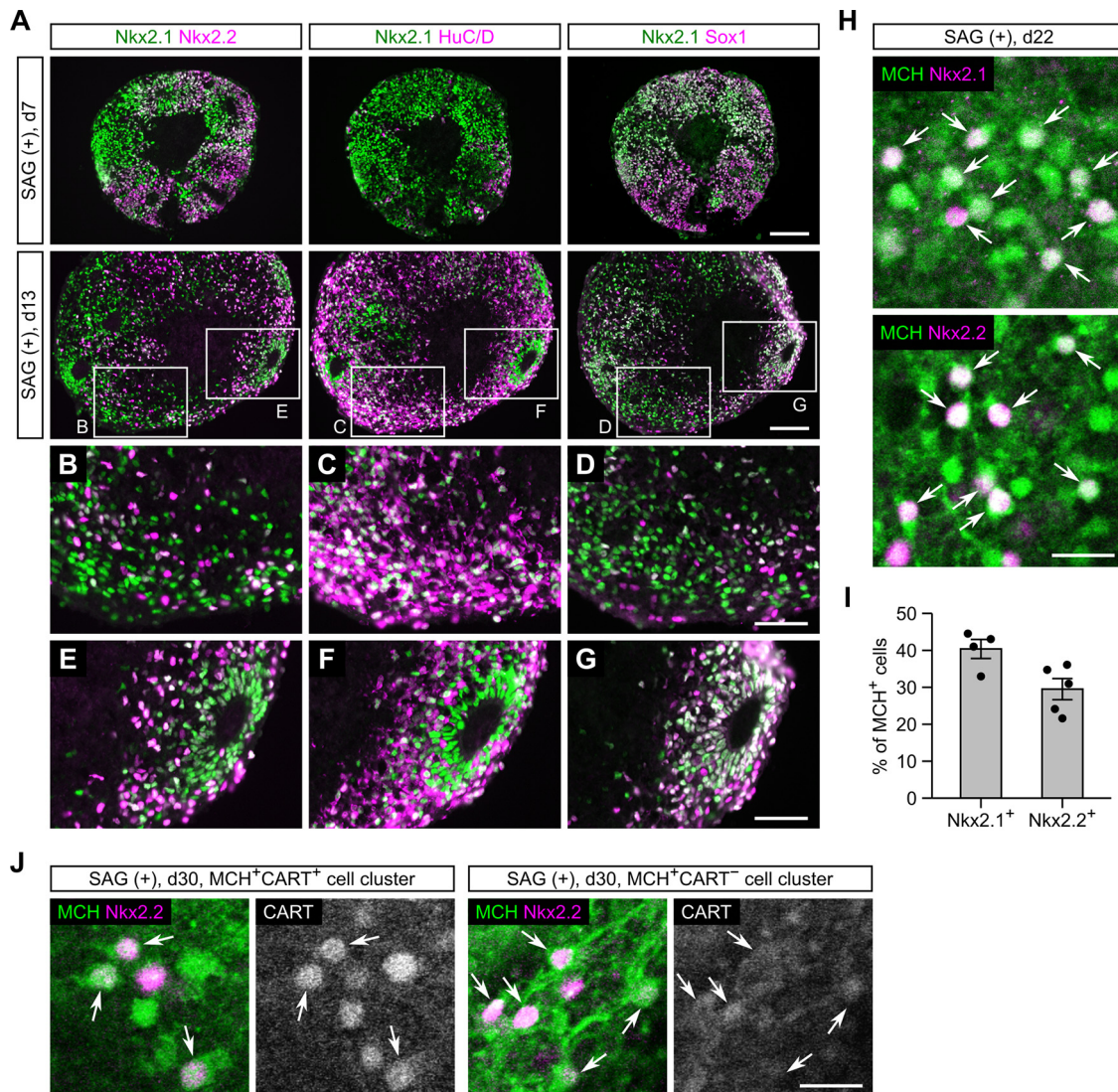


Figure 6. Characterization of neuronal differentiation in SAG-treated ES-Hypo. **A–G**, Serial sections from SFEBq-cultured mESC aggregates (with SAG) on days 7 and 13. The sections were immunostained for Nkx2.1/Nkx2.2 (#1), Nkx2.1/HuC/D (#2), or Nkx2.1/Sox1 (#3). The day-13 aggregate contains a HuC/D⁺ neuron-dense area (**B–D**) and a Sox1⁺ rosette structure (**E–G**). Scale bars: 100 μm (**A**) and 50 μm (**B–G**). **H**, Representative images of SAG-treated mESC aggregates immunostained for MCH/Nkx2.1 (top) and MCH/Nkx2.2 (bottom) on day 22. Arrows indicate double-positive cells. Scale bar: 20 μm . **I**, The percentage of MCH-ir cells expressing Nkx2.1 or Nkx2.2 on day 22. $n = 4–5$ aggregates per marker. **J**, Triple immunostaining of SAG-treated mESC aggregates for MCH/CART/Nkx2.2 on day 30. Representative images of MCH⁺CART⁺ (left) and MCH⁺CART⁻ (right) cell clusters are shown, and MCH⁺Nkx2.2⁺ cells are indicated by arrows. Scale bar: 20 μm .

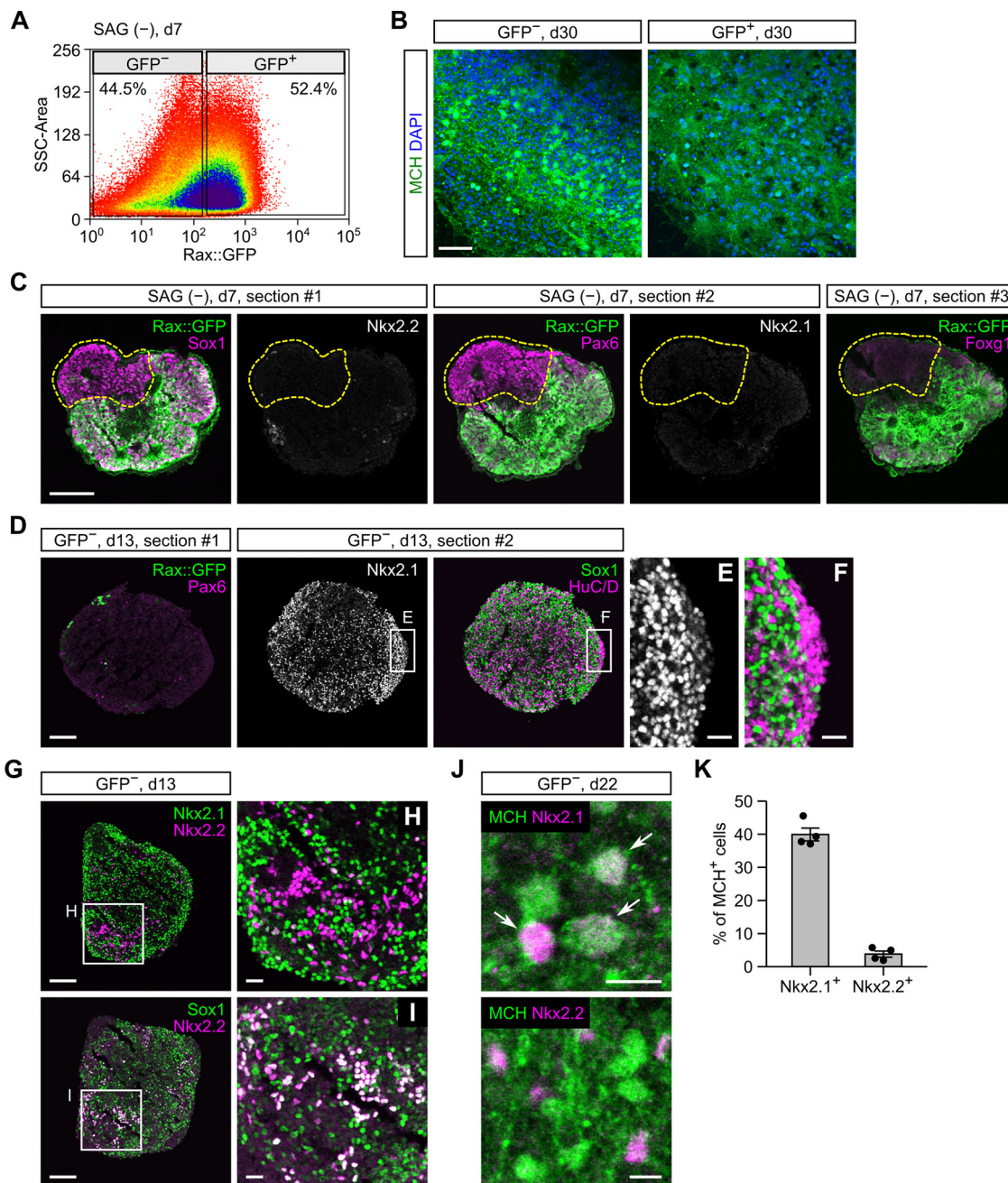


Figure 7. Characterization of neuronal differentiation in SAG-free ES-Hypo. **A**, FACS sorting of Rax::GFP⁺ and GFP⁻ cells from SFEBq-cultured mESC aggregates (without SAG) on day 7. **B**, Immunofluorescence images of Rax::GFP⁺ (right) and GFP⁻ (left) cell aggregates. FACS-sorted GFP⁺ and GFP⁻ cells were reaggregated and cultured until day 30 before staining for MCH. Nuclei were stained with DAPI. Scale bar: 50 μ m. **C**, Serial sections from a day-7 aggregate cultured without SAG. The sections were immunostained for GFP/Sox1/Nkx2.2 (#1), GFP/Pax6/Nkx2.1 (#2), or GFP/Foxg1 (#3). Scale bar: 100 μ m. **D–J**, Immunofluorescence analysis of GFP⁻ cell aggregates on days 13 and 22. Two serial sections from a day-13 aggregate were stained for GFP/Pax6 or Nkx2.1/Sox1/HuC/D (**D–F**). Two sections from a day-22 aggregate were stained for MCH/Nkx2.1 or MCH/Nkx2.2 (**J**, arrows indicate double-positive cells). Scale bars: 100 μ m (**D**, **G**), 20 μ m (**E**, **F**, **H**, **I**), and 10 μ m (**J**). **K**, The percentage of MCH-ir cells expressing Nkx2.1 or Nkx2.2 in GFP⁻ cell aggregates on day 22. $n = 4$ aggregates per marker.

generate both subtypes of MCH neurons in SAG-treated ES-Hypo.

We next tested SAG-free ES-Hypo. During first week of culture, many mESCs differentiate into Rax⁺Pax6⁺ progenitors (Fig. 5B,C). However, it is difficult to trace the

neuronal progeny of these progenitors because the expression of Rax/Pax6 was abolished in postmitotic cells in the hypothalamus (Wataya et al., 2008). We therefore performed FACS sorting of Rax::GFP⁺ and GFP⁻ cells on day 7 (Fig. 7A) to clarify whether Rax⁺Pax6⁺ progenitors

are capable of producing MCH neurons. Unexpectedly, we found that the GFP⁻ but not GFP⁺ cell fraction robustly generated MCH-ir cells after neuronal differentiation (Fig. 7B). On day 7, Rax::GFP⁻ cells expressed Sox1/Pax6 but not Nkx2.1/Nkx2.2/Foxg1 (Fig. 7C). This expression profile represents a subpopulation of dorsal hypothalamic progenitors (Wataya et al., 2008) or prethalamic progenitors (Fig. 5A). We further analyzed the neuronal differentiation of the sorted Rax::GFP⁻ cells (i.e., Rax⁻Pax6⁺ progenitors). The expression of Pax6 was almost completely abolished in the GFP⁻ cell aggregates on day 13, but surprisingly, a great number of Nkx2.1⁺ cells were observed in the same samples (Fig. 7D). These Nkx2.1⁺ cells contained Sox1⁺ neural progenitors and HuC/D⁺ postmitotic neurons (Fig. 7D–F). Both populations were contiguous or intermingled, indicating that Nkx2.1⁺HuC/D⁺ neurons were directly produced by Nkx2.1⁺Sox1⁺ progenitors. Because Nkx2.1-immunoreactivity in HuC/D⁺ neurons was weaker than in neighboring Sox1⁺ progenitors (Fig. 7E,F), Nkx2.1 seems downregulated on neuronal differentiation. Nevertheless, more than half of HuC/D⁺ neurons were detected as Nkx2.1⁺, suggesting that Rax⁻Pax6⁺ early progenitors contribute to neurogenesis by supplying Nkx2.1⁺ intermediate progenitors rather than producing neurons by themselves. We also observed a small number of Nkx2.2⁺ cells, but most of them were Nkx2.1⁻/Sox1⁺ (Fig. 7G–I) and therefore probably represent a progenitor population distinct from the Nkx2.1⁺ cell lineage. When GFP⁻ cell aggregates were cultured until day 22, the expression of Nkx2.1 was observed in 40% of MCH-ir cells but that of Nkx2.2 was limited to ~4% of MCH-ir cells (Fig. 7J,K). Taken together, our data suggest that MCH neurons can originate from Rax⁻Pax6⁺ early progenitors mainly through Nkx2.1⁺Nkx2.2⁻ intermediate progenitors in SAG-free ES-Hypo.

Discussion

MCH neurons are preferentially located in the LHA, but they have no well-defined territory and are intermingled with other cell groups, such as orexin neurons (Hahn, 2010). This organization makes it hard to predict the embryonic progenitor domain as well as the developmental signals (e.g., morphogens and transcriptional factors) allocated for MCH neurons. ES-Hypo can partially resolve this difficulty; it is usable for screening culture conditions to induce specific hypothalamic lineages in a systematic, stepwise manner, and such trials should provide crucial information on the lineage specification and maturation. In the present study, we used this approach to gain insight into the mechanism of MCH neuron development. We found that ES-Hypo can produce several MCH-ir neurons that reproduce well-known features of native MCH neurons. Most importantly, we uncovered that the major neurochemical subpopulations of MCH neurons, the CART⁺ and CART⁻ MCH neurons, are differentiated from mESCs under the influence of Hh signaling.

The original report on ES-Hypo was primarily focused on the culture conditions to specify Rax⁺ hypothalamic progenitors and did not fully examine the neuronal fates of the progenitors (Wataya et al., 2008). The authors described that the Rax⁺ progenitors bearing a dorsal or

ventral hypothalamic identity could generate vasopressin neurons or neurons observed in the ventromedial and arcuate nuclei of the hypothalamus, respectively. Subsequent reports have documented the occurrence of orexin neurons in ES-Hypo (Merkle et al., 2015) and its modified culture (Hayakawa et al., 2013); however, the present study provides the first characterization of MCH neurons in ES-Hypo. We found that a large fraction (37–81%) of neurons in ES-Hypo were immunopositive for MCH, regardless of whether ES-Hypo was derived from dorsal or ventral hypothalamic progenitors. This proportion seems to be much higher in comparison to previous reports on vasopressin neurons (6% of day-20 cells differentiated from Rax::GFP⁺ progenitors; Wataya et al., 2008). Indeed, we observed less copeptin-ir cells (copeptin is a peptide derived from the vasopressin precursor) in comparison to MCH-ir cells in ES-Hypo after four to five weeks of differentiation (data not shown). These data suggest that ES-Hypo generates a wide range of hypothalamic neurons, among which MCH neurons are a predominant population.

We examined the time course of neural progenitor specification and subsequent neurogenesis in ES-Hypo and showed that it follows the temporal pattern of fetal hypothalamic development. In addition to this overall similarity, MCH cells born in ES-Hypo reproduced morphologic changes observed *in vivo* for developing MCH neurons and acquired neurochemical phenotypes common to mature hypothalamic MCH neurons (the latter feature is discussed in detail below). Moreover, we found that orexin neurons developed later than MCH neurons in ES-Hypo and these cell groups appeared to form reciprocal connections. Both findings are reminiscent of native MCH and orexin neurons in the rodent hypothalamus (Bayer et al., 2002; Guan et al., 2002; Steininger et al., 2004; van den Pol et al., 2004; Díaz et al., 2014). Although it is unknown whether the MCH-orexin neuronal connections are specific to either of the subpopulations of MCH neurons *in vivo*, our results suggest that both CART⁺ and CART⁻ MCH neurons receive inputs from orexin neurons in ES-Hypo. A recent study succeeded in generating MCH and orexin neurons from mouse iPSCs using a culture protocol based on that for ES-Hypo (Seifinejad et al., 2019). The authors achieved neuronal differentiation within two weeks of culture by applying inductive factors, such as BMP7 and vitamin C, whereas we confirmed the generation of MCH and orexin neurons after longer culture of ES-Hypo without any inductive factors. Taken together, our data support the idea that ES-Hypo can recapitulate the developmental programs of MCH neurons and probably orexin neurons in an autonomous manner.

One of the most remarkable properties of native MCH neurons is their co-expression of multiple neurochemical molecules, including neuropeptides (CART and nesfatin-1) and markers for GABAergic and glutamatergic cells (GAD67 and VGLUT2). The expression of CART, nesfatin-1, and GAD67 in MCH neurons was previously detected at both mRNA and protein levels (Broberger, 1999; Vrang et al., 1999; Brailoiu et al., 2007; Sapin et al., 2010; Mickelsen et al., 2017; Noble et al., 2018). The expression

of VGLUT2 was found in nearly all MCH neurons using VGLUT2-GFP reporter mice, single-cell transcriptomics, and ISH (Chee et al., 2015; Mickelsen et al., 2017, 2019; Schneeberger et al., 2018; Naganuma et al., 2019; Hung et al., 2020). It has been reported that VGLUT2 deletion in MCH neurons affects glucose metabolism, food reward, and REM sleep in mice (Schneeberger et al., 2018; Naganuma et al., 2019), suggesting functional glutamate signaling by MCH neurons. On the other hand, another study using VGLUT2-tdTomato mice (generated by mating VGLUT2-Cre mice to Ai14 Cre reporter mice) failed to detect tdTomato signals in MCH neurons (Blanco-Centurion et al., 2018). Our results based on double immunofluorescence staining indicated that mESC-derived MCH neurons largely co-express CART, nesfatin-1, GAD67, and VGLUT2. The co-expression of these markers has been confirmed in native MCH neurons at mRNA levels (Mickelsen et al., 2017); however, to our knowledge, this is the first report to demonstrate the simultaneous presence of endogenous GAD67 and VGLUT2 proteins in MCH neurons. Although the functional consequences of this neurochemical multiplicity remain to be elucidated, it has been shown that native MCH neurons can release GABA (Jego et al., 2013) and glutamate (Chee et al., 2015), as well as MCH (Noble et al., 2018). Thus, the present study not only supports the neurochemical similarity between mESC-derived and native MCH neurons, but also provides additional evidence of the dual GABAergic-glutamatergic phenotype of MCH neurons.

The most striking finding of our study is that CART-negative MCH neurons substantially developed in ES-Hypo only when the Hh agonist SAG was added to the differentiation media. In the embryonic mouse brain, most MCH⁺CART⁻ neurons are born at the initial phase of neurogenesis (E9–E10) and followed by the generation of MCH⁺CART⁺ neurons (E11–E12; Croizier et al., 2010). This birth order is reflected in the final localization of those neurons in the adult brain. Earlier born MCH⁺CART⁻ neurons are predominantly located in the dorsal-lateral part of the caudal LHA close to the cerebellar peduncle, although a minor fraction of them are found in the perifornical region of the LHA at more caudal levels (Croizier et al., 2010). Later born MCH⁺CART⁺ neurons are mainly distributed in the rostral and medial hypothalamic portions, but also in additional locations, including the rostral zona incerta, the dorsal-lateral part of the caudal LHA, and the ventral capsule of the posterior hypothalamic nucleus (Croizier et al., 2010). It remains unknown whether these subtypes of MCH neurons originate from a common or distinct progenitors. On the other hand, a previous study has shown that early-born MCH⁺ cells in the E13–E15 rat brain appear to come from the Nkx2.1/Nkx2.2 co-expressing region in the caudal hypothalamic neuroepithelium (Croizier et al., 2011; Fig. 5A). The corresponding region is also proposed as an origin of early MCH cells in the fetal mouse brain (Díaz et al., 2014). Consistent with these *in vivo* data, SFEBq-cultured mESCs differentiated into Nkx2.1⁺Nkx2.2⁺ hypothalamic progenitors and then generated MCH neurons, including both CART⁺ and

CART⁻ cells, in the presence of SAG. Under this condition, most mESCs were specified into Nkx2.1⁺ ventral hypothalamic progenitors by Hh signaling, like the patterning event in the hypothalamic anlage (Xie and Dorsky, 2017). Only half of the Nkx2.1⁺ progenitors co-expressed Nkx2.2, but we observed co-localization of Nkx2.2 with both subtypes of MCH neurons after terminal differentiation. Based on this result, we concluded that Nkx2.1⁺Nkx2.2⁺ progenitors are an origin of both CART⁺ and CART⁻ MCH neurons in SAG-treated ES-Hypo. We cannot rule out the possibility that other types of neural progenitors also contribute to the production of MCH neurons, as the expression of Nkx2.1/Nkx2.2 was limited to 30–40% of MCH neurons (Fig. 6). However, the expression of the Nkx genes seems downregulated on terminal differentiation of MCH neurons (Croizier et al., 2011), suggesting that most MCH neurons are produced by Nkx2.1⁺Nkx2.2⁺ progenitors in the presence of SAG. It is currently unclear how Nkx2.1⁺Nkx2.2⁺ progenitors generate the two subtypes of MCH neurons. A plausible hypothesis is that CART⁻ and CART⁺ MCH neurons are derived from early and intermediate stages of Nkx2.1⁺Nkx2.2⁺ progenitors, respectively, according to the birth order for *in vivo* MCH neurons (Fig. 8). This idea is consistent with our observation that both subpopulations of MCH neurons were generally found in discrete clusters and not intermingled with each other in ES-Hypo (Fig. 5E). In this case, a stage-specific phenotype of Nkx2.1⁺Nkx2.2⁺ progenitors may determine the phenotype of their descendant MCH neurons. Alternatively, extracellular factors may influence late generated MCH neurons to express CART, as suggested previously (Cvetkovic et al., 2004).

In the present study, we only performed SAG treatment in a continuous manner (from day 4 onward) and therefore could not clarify whether Hh signaling has an effect not only on ventralizing hypothalamic progenitors but also on their subsequent terminal differentiation. In this respect, a genetic study has revealed that the elimination of the functional Shh expression in the developing diencephalon severely impairs the production of MCH neurons, especially in the LHA (Szabó et al., 2009), wherein MCH⁺CART⁻ neurons are predominantly localized. It has also been reported that the MCH mRNA level was decreased by 90% in E13 mouse embryos after pregnant mice were injected with an Hh inhibitor on E11 (Croizier et al., 2011), when most presumptive MCH⁺CART⁻ neurons have already been born in embryos (Croizier et al., 2010). These previous findings provide evidence that Hh signaling is required for terminal differentiation and/or survival of MCH⁺CART⁻ neurons.

Without SAG treatment, SFEBq-cultured mESCs differentiated into Rax⁺Pax6⁺ dorsal hypothalamic progenitors or Rax⁻Pax6⁺ dorsal hypothalamic/prethalamic progenitors within the first week of culture. Under this condition, terminally differentiated MCH neurons were almost completely CART⁺. Through FACS sorting and subsequent differentiation analysis, we found that Rax⁻Pax6⁺ progenitors are an early origin of MCH⁺CART⁺ neurons in SAG-free ES-Hypo. These early progenitors next generate the second form of neural progenitors (Nkx2.1⁺Nkx2.2⁻),

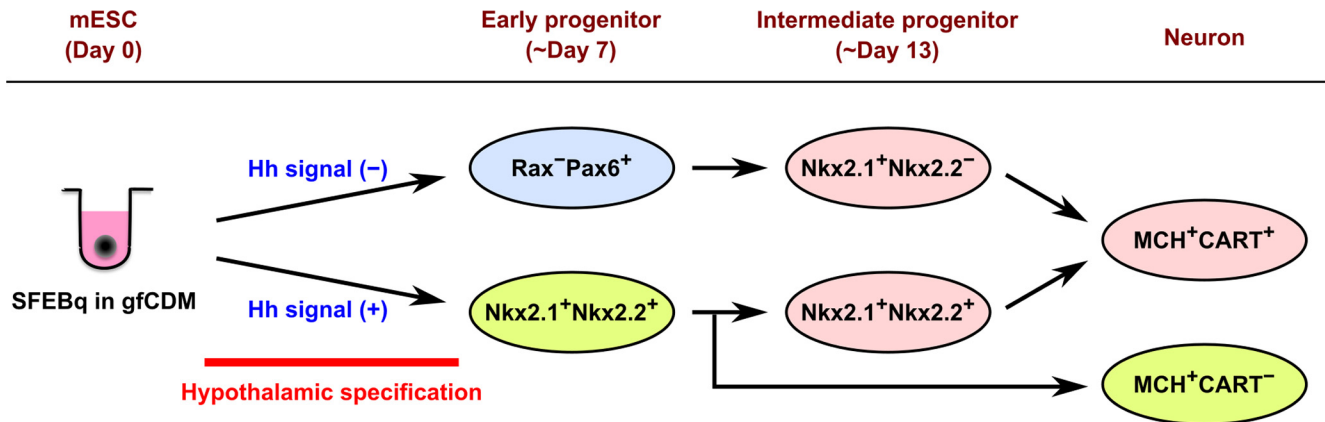


Figure 8. Schematic diagram of the different progenitor origins of MCH neurons suggested in the current study. SFEBq culture of mESCs in gfCDM with or without exogenous Hh signals can generate $Nkx2.1^+Nkx2.2^+$ ventral hypothalamic progenitors or Rax^-Pax6^+ dorsal hypothalamic/prethalamic progenitors, respectively, within a week. The $Nkx2.1^+Nkx2.2^+$ early progenitors directly produce MCH^+CART^- neurons and $Nkx2.1^+Nkx2.2^-$ intermediate progenitors, the latter of which generate MCH^+CART^+ neurons. The Rax^-Pax6^+ early progenitors also differentiate into MCH^+CART^+ neurons through $Nkx2.1^+Nkx2.2^-$ intermediate progenitors.

and this group of intermediate progenitors directly produces MCH neurons (Fig. 8). Although the regional identity of these intermediate progenitors remains unclear, a possible candidate is the perimammillary/periretromammillary (PM/PRM) region in the prosomeric hypothalamic model (Díaz et al., 2014). This region was identified as the second site of occurrence of MCH^+ cells, more ventral to the first site (i.e., the $Nkx2.1/Nkx2.2$ -positive region), by using the Allen Developmental Mouse Brain Atlas (Díaz et al., 2014). The PRM/PM area expresses $Nkx2.1$ but not $Nkx2.2$ (Díaz et al., 2014), consistent with the phenotype of the intermediate progenitors identified in SAG-free ES-Hypo.

In summary, we propose three different progenitor origins of MCH neurons in ES-Hypo (Fig. 8): (1) $Nkx2.1^+Nkx2.2^+$ early progenitors, (2) $Nkx2.1^+Nkx2.2^-$ intermediate progenitors, and (3) $Nkx2.1^+Nkx2.2^+$ intermediate progenitors. The first group selectively produces CART-negative MCH neurons, and the others CART-positive MCH neurons. The multiple progenitor origins of MCH neurons can be supported by recent transcriptome studies. Kim et al. (2020) performed clustering of embryonic mouse LHA cells (at E11–E13) using single-cell RNA-sequencing and identified 13 subclusters of young postmitotic neurons. Among them, five subclusters expressed both MCH and CART mRNAs and one subcluster MCH mRNA alone, implying that MCH neurons develop through multiple pathways. A similar transcriptional diversity was also found in hypothalamic POMC precursors (immature POMC⁺ neurons), and it was shown that distinct subclusters of POMC precursors finally develop into different phenotypes of arcuate neurons (Yu et al., 2022). In light of these findings, it is plausible that CART⁺ and CART⁻ MCH neurons are developed from distinct progenitors. Our results also suggested that CART-positive MCH neurons originate from two distinct progenitor lineages, which are specified in the presence or absence of Hh signaling (Fig. 8). This may account for the relatively wide distribution of MCH^+CART^+ neurons compared with MCH^+CART^- neurons in the adult

brain. Further studies, using a lineage tracing approach are needed to better understand the ontogeny of MCH neurons.

Another notable effect of SAG on ES-Hypo was the increased production of orexin neurons. Orexin-ir cells were observed only occasionally in the absence of SAG but were more reproducibly observed in the SAG-treated samples. Although the ontogeny of orexin neurons remains largely unknown, the LIM homeobox transcription factor *Lhx9* has been identified as a critical inducer of the orexin neuron specification in zebrafish and developing mice (Dalal et al., 2013; Liu et al., 2015). In the latter species, the expression of *Lhx9* occurs in the mantle layer of the tuberal hypothalamus during the neurogenic period and then colocalizes with a subset of orexin neurons in the LHA (Rétaux et al., 1999; Shimogori et al., 2010; Sokolowski et al., 2015). It has also been revealed that *Shh* signaling is indispensable for the development of orexin neurons as well as *Lhx9*⁺ cells in the mouse hypothalamus (Szabó et al., 2009; Shimogori et al., 2010). These previous data and our current findings strongly suggest that orexin neurons primarily arise from ventral hypothalamic progenitors under the control of Hh signaling. In this view, the stochastic induction of orexin cells without SAG is attributable to a small number of $Nkx2.1^+$ progenitors (Fig. 5B,C). In comparison to the abundant production of MCH neurons in ES-Hypo, the number of co-existing orexin neurons was much smaller, even in the presence of SAG (<15 cells on day 30). In rodents, most MCH neurons appear before birth; however, the number of orexin neurons as well as orexin immunoreactivity increase in the postnatal period (Yamamoto et al., 2000; Steininger et al., 2004; Ogawa et al., 2017). These observations suggest that the generation of orexin neurons in ES-Hypo may be promoted by extending the culture period in addition to SAG treatment. However, with more than five weeks of mESC differentiation, there was a massive expansion of residual undifferentiated cells, which

negatively affected the survival of differentiated neurons (data not shown).

In conclusion, ES-Hypo can recapitulate the developmental process of MCH neurons *in vitro* and therefore be a powerful tool to dissect the molecular mechanisms underlying this process. We also demonstrated that the Hh signaling pathway is a key organizer of the CART⁺ and CART⁻ subpopulations of MCH neurons. These neurochemical subpopulations have also been found in the human hypothalamus (Menyhárt et al., 2007). Hence, future comparative studies on MCH neurons derived from rodent and human stem cell lines may help clarify whether Hh signaling plays a conserved role in establishing the heterogeneity of MCH neurons in mammals.

References

- Apergis-Schoute J, Iordanidou P, Faure C, Jegou S, Schöne C, Aitta-Aho T, Adamantidis A, Burdakov D (2015) Optogenetic evidence for inhibitory signaling from orexin to MCH neurons via local microcircuits. *J Neurosci* 35:5435–5441.
- Bayer L, Mairet-Coello G, Risold P-Y, Griffond B (2002) Orexin/hypocretin neurons: chemical phenotype and possible interactions with melanin-concentrating hormone neurons. *Regul Pept* 104:33–39.
- Bittencourt JC, Presse F, Arias C, Peto C, Vaughan J, Nahon JL, Vale W, Sawchenko PE (1992) The melanin-concentrating hormone system of the rat brain: an immuno- and hybridization histochemical characterization. *J Comp Neurol* 319:218–245.
- Blanco-Centurion C, Bendell E, Zou B, Sun Y, Shiromani PJ, Liu M (2018) VGAT and VGLUT2 expression in MCH and orexin neurons in double transgenic reporter mice. *IBRO Rep* 4:44–49.
- Blanco-Centurion C, Luo S, Spergel DJ, Vidal-Ortiz A, Oprisan SA, Van den Pol AN, Liu M, Shiromani PJ (2019) Dynamic network activation of hypothalamic MCH neurons in REM sleep and exploratory behavior. *J Neurosci* 39:4986–4998.
- Brailoiu GC, Dun SL, Brailoiu E, Inan S, Yang J, Chang JK, Dun NJ (2007) Nesfatin-1: distribution and interaction with a G protein-coupled receptor in the rat brain. *Endocrinology* 148:5088–5094.
- Brischoux F, Fellmann D, Risold PY (2001) Ontogenetic development of the diencephalic MCH neurons: a hypothalamic “MCH area” hypothesis. *Eur J Neurosci* 13:1733–1744.
- Brischoux F, Cvetkovic V, Griffond B, Fellmann D, Risold PY (2002) Time of genesis determines projection and neurokinin-3 expression patterns of diencephalic neurons containing melanin-concentrating hormone. *Eur J Neurosci* 16:1672–1680.
- Broberger C (1999) Hypothalamic cocaine- and amphetamine-regulated transcript (CART) neurons: histochemical relationship to thyrotropin-releasing hormone, melanin-concentrating hormone, orexin/hypocretin and neuropeptide Y. *Brain Res* 848:101–113.
- Chee MJS, Arrigoni E, Maratos-Flier E (2015) Melanin-concentrating hormone neurons release glutamate for feedforward inhibition of the lateral septum. *J Neurosci* 35:3644–3651.
- Concetti C, Bracey EF, Peleg-Raibstein D, Burdakov D (2020) Control of fear extinction by hypothalamic melanin-concentrating hormone-expressing neurons. *Proc Natl Acad Sci U S A* 117:22514–22521.
- Conductier G, Brau F, Viola A, Langlet F, Ramkumar N, Dehouck B, Lemaire T, Chapot R, Lucas L, Rovère C, Maitre PY, Hosseiny S, Petit-Paitel A, Adamantidis A, Lakaye B, Risold PY, Prévot V, Meste O, Nahon JL, Guyon A (2013) Melanin-concentrating hormone regulates beat frequency of ependymal cilia and ventricular volume. *Nat Neurosci* 16:845–847.
- Croizier S, Franchi-Bernard G, Colard C, Poncet F, La Roche A, Risold P-Y (2010) A comparative analysis shows morphofunctional differences between the rat and mouse melanin-concentrating hormone systems. *PLoS One* 5:e15471.
- Croizier S, Amiot C, Chen X, Presse F, Nahon J-L, Wu JY, Fellmann D, Risold P-Y (2011) Development of posterior hypothalamic neurons enlightens a switch in the prosencephalic basic plan. *PLoS One* 6:e28574.
- Cvetkovic V, Brischoux F, Jacquemard C, Fellmann D, Griffond B, Risold P-Y (2004) Characterization of subpopulations of neurons producing melanin-concentrating hormone in the rat ventral diencephalon. *J Neurochem* 91:911–919.
- Dalal J, Roh JH, Maloney SE, Akuffo A, Shah S, Yuan H, Wamsley B, Jones WB, de Guzman Strong C, Gray PA, Holtzman DM, Heintz N, Dougherty JD (2013) Translational profiling of hypocretin neurons identifies candidate molecules for sleep regulation. *Genes Dev* 27:565–578.
- Diaz C, Morales-Delgado N, Puelles L (2014) Ontogenesis of peptidergic neurons within the genoarchitectonic map of the mouse hypothalamus. *Front Neuroanat* 8:162.
- Dilsiz P, Aklan I, Sayar Atasoy N, Yavuz Y, Filiz G, Koksalar F, Ates T, Oncul M, Coban I, Ates Oz E, Cebecioglu U, Alp MI, Yilmaz B, Atasoy D (2020) MCH neuron activity is sufficient for reward and reinforces feeding. *Neuroendocrinology* 110:258–270.
- Diniz GB, Bittencourt JC (2017) The melanin-concentrating hormone as an integrative peptide driving motivated behaviors. *Front Syst Neurosci* 11:32.
- Diniz GB, Battagello DS, Cherubini PM, Reyes-Mendoza JD, Luna-Illades C, Klein MO, Motta-Teixeira LC, Sita LV, Miranda-Anaya M, Morales T, Bittencourt JC (2019) Melanin-concentrating hormone peptidergic system: comparative morphology between muroid species. *J Comp Neurol* 527:2973–3001.
- Domingos AI, Sordillo A, Dietrich MO, Liu Z-W, Tellez LA, Vaynshteyn J, Ferreira JG, Ekstrand MI, Horvath TL, de Araujo IE, Friedman JM (2013) Hypothalamic melanin concentrating hormone neurons communicate the nutrient value of sugar. *Elife* 2:e01462.
- Esclapez M, Tillakaratne NJ, Kaufman DL, Tobin AJ, Houser CR (1994) Comparative localization of two forms of glutamic acid decarboxylase and their mRNAs in rat brain supports the concept of functional differences between the forms. *J Neurosci* 14:1834–1855.
- Ferran JL, Puelles L, Rubenstein JLR (2015) Molecular codes defining rostrocaudal domains in the embryonic mouse hypothalamus. *Front Neuroanat* 9:46.
- Foo KS, Brismar H, Broberger C (2008) Distribution and neuropeptide coexistence of nucleobindin-2 mRNA/nesfatin-like immunoreactivity in the rat CNS. *Neuroscience* 156:563–579.
- Fort P, Salvat D, Hanriot L, Jegou S, Shimizu H, Hashimoto K, Mori M, Luppi P-H (2008) The satiety molecule nesfatin-1 is co-expressed with melanin concentrating hormone in tuberal hypothalamic neurons of the rat. *Neuroscience* 155:174–181.
- Furukawa T, Kozak CA, Cepko CL (1997) rax, a novel paired-type homeobox gene, shows expression in the anterior neural fold and developing retina. *Proc Natl Acad Sci U S A* 94:3088–3093.
- Guan JL, Uehara K, Lu S, Wang QP, Funahashi H, Sakurai T, Yanagizawa M, Shioda S (2002) Reciprocal synaptic relationships between orexin- and melanin-concentrating hormone-containing neurons in the rat lateral hypothalamus: a novel circuit implicated in feeding regulation. *Int J Obes Relat Metab Disord* 26:1523–1532.
- Hahn JD (2010) Comparison of melanin-concentrating hormone and hypocretin/orexin peptide expression patterns in a current parceling scheme of the lateral hypothalamic zone. *Neurosci Lett* 468:12–17.
- Hanriot L, Camargo N, Courau AC, Leger L, Luppi PH, Peyron C (2007) Characterization of the melanin-concentrating hormone neurons activated during paradoxical sleep hypersomnia in rats. *J Comp Neurol* 505:147–157.
- Hassani OK, Lee MG, Jones BE (2009) Melanin-concentrating hormone neurons discharge in a reciprocal manner to orexin neurons across the sleep-wake cycle. *Proc Natl Acad Sci U S A* 106:2418–2422.
- Hayakawa K, Hirokawa M, Tabei Y, Arai D, Tanaka S, Murakami N, Yagi S, Shiota K (2013) Epigenetic switching by the metabolism-

- sensing factors in the generation of orexin neurons from mouse embryonic stem cells. *J Biol Chem* 288:17099–17110.
- Hung CJ, Ono D, Kilduff TS, Yamanaka A (2020) Dual orexin and MCH neuron-ablated mice display severe sleep attacks and catalepsy. *Elife* 9:e54275.
- Ishii Y, Bouret SG (2012) Embryonic birthdate of hypothalamic leptin-activated neurons in mice. *Endocrinology* 153:3657–3667.
- Izawa S, Chowdhury S, Miyazaki T, Mukai Y, Ono D, Inoue R, Ohmura Y, Mizoguchi H, Kimura K, Yoshioka M, Terao A, Kilduff TS, Yamanaka A (2019) REM sleep-active MCH neurons are involved in forgetting hippocampus-dependent memories. *Science* 365:1308–1313.
- Jego S, Glasgow SD, Herrera CG, Ekstrand M, Reed SJ, Boyce R, Friedman J, Burdakov D, Adamantidis AR (2013) Optogenetic identification of a rapid eye movement sleep modulatory circuit in the hypothalamus. *Nat Neurosci* 16:1637–1643.
- Kasai T, et al. (2020) Hypothalamic contribution to pituitary functions is recapitulated in vitro using 3D-cultured human iPSC cells. *Cell Rep* 30:18–24.e5.
- Kim DW, Washington PW, Wang ZQ, Lin SH, Sun C, Ismail BT, Wang H, Jiang L, Blackshaw S (2020) The cellular and molecular landscape of hypothalamic patterning and differentiation from embryonic to late postnatal development. *Nat Commun* 11:4360.
- Komagata N, Latifi B, Rusterholz T, Bassetti CLA, Adamantidis A, Schmidt MH (2019) Dynamic REM sleep modulation by ambient temperature and the critical role of the melanin-concentrating hormone system. *Curr Biol* 29:1976–1987.e4.
- Konadhode RR, Pelluru D, Blanco-Centurion C, Zayachkivsky A, Liu M, Uhde T, Glen WB Jr, van den Pol AN, Mulholland PJ, Shiromani PJ (2013) Optogenetic stimulation of MCH neurons increases sleep. *J Neurosci* 33:10257–10263.
- Konadhode RR, Pelluru D, Shiromani PJ (2014) Neurons containing orexin or melanin concentrating hormone reciprocally regulate wake and sleep. *Front Syst Neurosci* 8:244.
- Kosse C, Burdakov D (2019) Natural hypothalamic circuit dynamics underlying object memorization. *Nat Commun* 10:2505.
- Li S, Yip A, Bird J, Seok BS, Chan A, Godden KE, Tam LD, Ghelardoni S, Balaban E, Martinez-Gonzalez D, Pompeiano M (2018) Melanin-concentrating hormone (MCH) neurons in the developing chick brain. *Brain Res* 1700:19–30.
- Liu J, Merkle FT, Gandhi AV, Gagnon JA, Woods IG, Chiu CN, Shimogori T, Schier AF, Prober DA (2015) Evolutionarily conserved regulation of hypocretin neuron specification by Lhx9. *Development* 142:1113–1124.
- Lu F, Kar D, Gruenig N, Zhang ZW, Cousins N, Rodgers HM, Swindell EC, Jamrich M, Schuurmans C, Mathers PH, Kurrasch DM (2013) Rax is a selector gene for mediobasal hypothalamic cell types. *J Neurosci* 33:259–272.
- Marín O, Baker J, Puelles L, Rubenstein JLR (2002) Patterning of the basal telencephalon and hypothalamus is essential for guidance of cortical projections. *Development* 129:761–773.
- Mathers PH, Grinberg A, Mahon KA, Jamrich M (1997) The Rx homeobox gene is essential for vertebrate eye development. *Nature* 387:603–607.
- Menyhárt J, Wittmann G, Lechan RM, Keller E, Liposits Z, Fekete C (2007) Cocaine- and amphetamine-regulated transcript (CART) is colocalized with the orexigenic neuropeptide Y and agouti-related protein and absent from the anorexigenic α -melanocyte-stimulating hormone neurons in the infundibular nucleus of the human hypothalamus. *Endocrinology* 148:4276–4281.
- Merkle FT, Maroof A, Wataya T, Sasai Y, Studer L, Eggan K, Schier AF (2015) Generation of neuropeptidergic hypothalamic neurons from human pluripotent stem cells. *Development* 142:633–643.
- Mickelsen LE, Kolling FW 4th, Chimileski BR, Fujita A, Norris C, Chen K, Nelson CE, Jackson AC (2017) Neurochemical heterogeneity among lateral hypothalamic hypocretin/orexin and melanin-concentrating hormone neurons identified through single-cell gene expression analysis. *eNeuro* 4:ENEURO.0013-17.2017.
- Mickelsen LE, Bolisetty M, Chimileski BR, Fujita A, Beltrami EJ, Costanzo JT, Naparstek JR, Robson P, Jackson AC (2019) Single-cell transcriptomic analysis of the lateral hypothalamic area reveals molecularly distinct populations of inhibitory and excitatory neurons. *Nat Neurosci* 22:642–656.
- Naganuma F, Bandaru SS, Absi G, Chee MJ, Vetrivelan R (2019) Melanin-concentrating hormone neurons promote rapid eye movement sleep independent of glutamate release. *Brain Struct Funct* 224:99–110.
- Noble EE, Hahn JD, Konanur VR, Hsu TM, Page SJ, Cortella AM, Liu CM, Song MY, Suarez AN, Szujewski CC, Rider D, Clarke JE, Darvas M, Appleyard SM, Kanoski SE (2018) Control of feeding behavior by cerebral ventricular volume transmission of melanin-concentrating hormone. *Cell Metab* 28:55–68.e7.
- Ogawa Y, Kanda T, Vogt K, Yanagisawa M (2017) Anatomical and electrophysiological development of the hypothalamic orexin neurons from embryos to neonates. *J Comp Neurol* 525:3809–3820.
- Ogawa K, Suga H, Ozone C, Sakakibara M, Yamada T, Kano M, Mitsumoto K, Kasai T, Kodani Y, Nagasaki H, Yamamoto N, Hagiwara D, Goto M, Banno R, Sugimura Y, Arima H (2018) Vasopressin-secreting neurons derived from human embryonic stem cells through specific induction of dorsal hypothalamic progenitors. *Sci Rep* 8:3615.
- Rajamani U, Gross AR, Hjelm BE, Sequeira A, Vawter MP, Tang J, Gangalapudi V, Wang Y, Andres AM, Gottlieb RA, Sareen D (2018) Super-obese patient-derived iPSC hypothalamic neurons exhibit obesogenic signatures and hormone responses. *Cell Stem Cell* 22:698–712.e9.
- Rao Y, Lu M, Ge F, Marsh DJ, Qian S, Wang AH, Picciotto MR, Gao XB (2008) Regulation of synaptic efficacy in hypocretin/orexin-containing neurons by melanin concentrating hormone in the lateral hypothalamus. *J Neurosci* 28:9101–9110.
- Rétaux S, Rogard M, Bach I, Failli V, Besson M-J (1999) Lhx9: a novel LIM-homeodomain gene expressed in the developing forebrain. *J Neurosci* 19:783–793.
- Saito Y, Cheng M, Leslie FM, Civelli O (2001) Expression of the melanin-concentrating hormone (MCH) receptor mRNA in the rat brain. *J Comp Neurol* 435:26–40.
- Sapin E, Bérød A, Léger L, Herman PA, Luppi P-H, Peyron C (2010) A very large number of GABAergic neurons are activated in the tuberal hypothalamus during paradoxical (REM) sleep hypersomnia. *PLoS One* 5:e11766.
- Schindelin J, Arganda-Carreras I, Frise E, Kaynig V, Longair M, Pietzsch T, Preibisch S, Rueden C, Saalfeld S, Schmid B, Tinevez J-Y, White DJ, Hartenstein V, Eliceiri K, Tomancak P, Cardona A (2012) Fiji: an open-source platform for biological-image analysis. *Nat Methods* 9:676–682.
- Schneeberger M, Tan K, Nectow AR, Parolari L, Caglar C, Azevedo E, Li Z, Domingos A, Friedman JM (2018) Functional analysis reveals differential effects of glutamate and MCH neuropeptide in MCH neurons. *Mol Metab* 13:83–89.
- Seifinejad A, Li S, Mikhail C, Vassalli A, Pradervand S, Arribat Y, Modarres HP, Allen B, John RM, Amati F, Tafti M (2019) Molecular codes and in vitro generation of hypocretin and melanin concentrating hormone neurons. *Proc Natl Acad Sci USA* 116:17061–17070.
- Shimada M, Nakamura T (1973) Time of neuron origin in mouse hypothalamic nuclei. *Exp Neurol* 41:163–173.
- Shimamura K, Hartigan DJ, Martinez S, Puelles L, Rubenstein JL (1995) Longitudinal organization of the anterior neural plate and neural tube. *Development* 121:3923–3933.
- Shimogori T, Lee DA, Miranda-Angulo A, Yang Y, Wang H, Jiang L, Yoshida AC, Kataoka A, Mashiko H, Avetisyan M, Qi L, Qian J, Blackshaw S (2010) A genomic atlas of mouse hypothalamic development. *Nat Neurosci* 13:767–775.
- Sokolowski K, Esumi S, Hirata T, Kamal Y, Tran T, Lam A, Oboti L, Brighaupt S-C, Zaghlula M, Martinez J, Ghimbovski S, Knobloch S, Pierani A, Tamamaki N, Shah NM, Jones KS, Corbin JG (2015) Specification of select hypothalamic circuits and innate behaviors by the embryonic patterning gene *dbx1*. *Neuron* 86:403–416.

- Soya S, Sakurai T (2020) Evolution of orexin neuropeptide system: structure and function. *Front Neurosci* 14:691.
- Steininger TL, Kilduff TS, Behan M, Benca RM, Landry CF (2004) Comparison of hypocretin/orexin and melanin-concentrating hormone neurons and axonal projections in the embryonic and postnatal rat brain. *J Chem Neuroanat* 27:165–181.
- Szabó NE, Zhao T, Cankaya M, Theil T, Zhou X, Alvarez-Bolado G (2009) Role of neuroepithelial sonic hedgehog in hypothalamic patterning. *J Neurosci* 29:6989–7002.
- Tortorello P, Sampogna S, Morales FR, Chase MH (2006) MCH-containing neurons in the hypothalamus of the cat: searching for a role in the control of sleep and wakefulness. *Brain Res* 1119:101–114.
- van den Pol AN, Acuna-Goycolea C, Clark KR, Ghosh PK (2004) Physiological properties of hypothalamic MCH neurons identified with selective expression of reporter gene after recombinant virus infection. *Neuron* 42:635–652.
- Vas S, Ádori C, Könczöl K, Kátai Z, Pap D, Papp RS, Bagdy G, Palkovits M, Tóth ZE (2013) Nesfatin-1/NUCB2 as a potential new element of sleep regulation in rats. *PLoS One* 8:e59809.
- Vetrivelan R, Kong D, Ferrari LL, Arrigoni E, Madara JC, Bandaru SS, Lowell BB, Lu J, Saper CB (2016) Melanin-concentrating hormone neurons specifically promote rapid eye movement sleep in mice. *Neuroscience* 336:102–113.
- Vrang N, Larsen PJ, Clausen JT, Kristensen P (1999) Neurochemical characterization of hypothalamic cocaine- amphetamine-regulated transcript neurons. *J Neurosci* 19:RC5.
- Wang L, Meece K, Williams DJ, Lo KA, Zimmer M, Heinrich G, Martin Carli J, Leduc CA, Sun L, Zeltser LM, Freeby M, Goland R, Tsang SH, Wardlaw SL, Egli D, Leibel RL (2015) Differentiation of hypothalamic-like neurons from human pluripotent stem cells. *J Clin Invest* 125:796–808.
- Wataya T, Ando S, Muguruma K, Ikeda H, Watanabe K, Eiraku M, Kawada M, Takahashi J, Hashimoto N, Sasai Y (2008) Minimization of exogenous signals in ES cell culture induces rostral hypothalamic differentiation. *Proc Natl Acad Sci USA* 105:11796–11801.
- Xie Y, Dorsky RI (2017) Development of the hypothalamus: conservation, modification and innovation. *Development* 144:1588–1599.
- Xie Y, Kaufmann D, Moulton MJ, Panahi S, Gaynes JA, Watters HN, Zhou D, Xue H-H, Fung CM, Levine EM, Letsou A, Brennan KC, Dorsky RI (2017) Lef1-dependent hypothalamic neurogenesis inhibits anxiety. *PLoS Biol* 15:e2002257.
- Yamamoto Y, Ueta Y, Hara Y, Serino R, Nomura M, Shibuya I, Shirahata A, Yamashita H (2000) Postnatal development of orexin/hypocretin in rats. *Brain Res Mol Brain Res* 78:108–119.
- Yu H, Rubinstein M, Low MJ (2022) Developmental single-cell transcriptomics of hypothalamic POMC neurons reveal the genetic trajectories of multiple neuropeptidergic phenotypes. *Elife* 11:e72883.